Review | Open Access

Energy Materials

Cui et al. Energy Mater. 2026, 6, 600063 DOI:10.20517/energymater.2026.30

Ion-concentration gradient electrolyte engineering in aqueous Zn-based batteries

Yifan Cui[1,*], Zhenlong Jin[1], Xinling Yu[1], Yi He[2,*], Xulai Yang[1,*]

Keywords:
Aqueous Zn-based batteries, quasi/all solid-state batteries, Zn electrode, gradient electrolyte, advanced characterization

Citation: Cui, Y.; Jin, Z.; Yu, X.; He, Y.; Yang, X. Ion-concentration gradient electrolyte engineering in aqueous Zn-based batteries. *Energy Mater.* **2026**, *6*, 600063. https://dx.doi.org/10.20517/energymater.2026.30

Received: 7 Mar 2026
First Decision: 16 Apr 2026
Revised: 3 May 2026
Accepted: 4 Jun 2026
Published: 17 Jun 2026

Academic Editor: Bin Wang
Copy Editor: Fangling Lan
Production Editor: Fangling Lan

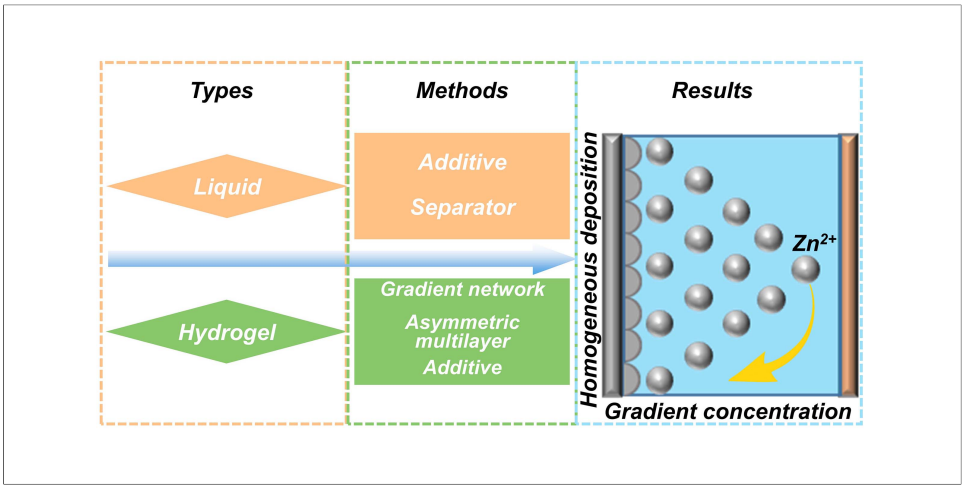

Abstract

Aqueous Zn-based batteries (AZBs) have attracted considerable attention as promising energy storage systems because of their intrinsic safety, low cost, and environmental friendliness. However, their practical application is limited by the instability of the Zn electrode interface, including uneven Zn deposition, hydrogen evolution, and other parasitic side reactions. These issues are closely related to the heterogeneous distribution of Zn^{2+} ions and the resulting imbalance of interfacial reactions during cycling. Ion concentration gradient engineering has therefore emerged as an effective strategy to regulate Zn^{2+} transport behavior and stabilize the Zn electrode interface. This review systematically summarizes recent advances in the construction of Zn^{2+} concentration gradients in AZBs, covering both liquid and hydrogel electrolyte systems. Representative strategies, including functional electrolyte additives, ion-selective separators, asymmetric electrolyte configurations, gradient hydrogel networks, and additive-assisted hydrogel electrolytes, are discussed. These approaches demonstrate that spatial regulation of Zn^{2+} concentration fields can fundamentally influence ion transport pathways, solvation and desolvation processes, electric double layer structures, and interfacial reaction kinetics, thereby homogenizing Zn^{2+} flux, suppressing hydrogen evolution and dendrite growth, and

[1]School of Advanced Manufacturing Engineering, LIB Technology Center of Anhui Province, Hefei University, Hefei 230601, Anhui, China.
[2]Department of Chemical Engineering, Waterloo Institute for Nanotechnology, University of Waterloo, Waterloo, ON N2L 3G1 Canada.

*Correspondence to: Dr. Yi He, Department of Chemical Engineering, Waterloo Institute for Nanotechnology, University of Waterloo, 200 University Avenue West, Waterloo, ON N2L 3G1 Canada. E-mail: yi.he@uwaterloo.ca; Dr. Yifan Cui, Dr. Xulai Yang, School of Advanced Manufacturing Engineering, LIB Technology Center of Anhui Province, Hefei University, Hefei 230601, Anhui, China. E-mail: cuiyf@hfuu.edu.cn; yangxl@hfuu.edu.cn

improving the reversibility of Zn plating and stripping. In addition, recent progress in advanced characterization techniques, including electrochemically parameterized ion transport modelling, *in situ* ion concentration mapping, and fluorescence-based operando visualization, is needed to elucidate the dynamic evolution of Zn^{2+} concentration gradients and their correlation with interfacial stability. Finally, general design principles, key challenges, and future perspectives for ion concentration gradient engineering are discussed, guiding the rational development of high-performance and durable AZBs.

INTRODUCTION

Aqueous Zn-based batteries (AZBs) have emerged as among the most promising next-generation electrochemical energy-storage technologies, driven by the increasing demand for devices that are not only highly energy dense but also intrinsically safe, cost effective, and environmentally sustainable[1-4] [Figure 1]. Compared with lithium-, sodium-, and other metal-ion-based batteries employing flammable organic electrolytes, AZBs capitalize on the intrinsic nonflammability and benign nature of water, offering a significantly enhanced safety profile suitable for large-scale grid energy storage and consumer electronics applications[5-10]. Zn metal further has this advantage: it is earth abundant, inexpensive, and environmentally compatible, and it has a high theoretical capacity (820 mAh g^{-1}) and low redox potential (-0.76 V *vs*. SHE)[11-13]. In addition, AZBs benefit from several practical advantages that make them particularly attractive for large-scale energy storage applications. The use of water-based electrolytes provides intrinsic safety compared with flammable organic electrolytes used in conventional lithium-ion batteries, significantly reducing the risks of thermal runaway and combustion. Zn is widely available in the Earth's crust and can be produced at low cost through mature metallurgical processes, supported by a well-established industrial infrastructure for Zn mining, refining, and recycling. These features collectively enable potentially low manufacturing costs and strong sustainability for grid-scale energy storage technologies.

Despite these compelling advantages, several intrinsic scientific challenges still hinder the practical deployment and commercial scalability of AZBs, including dendrite formation[14-21], electrode passivation[22-26], and the hydrogen evolution reaction (HER)[27-33]. Among them, uncontrolled Zn dendrite formation stands out as a key bottleneck, as it can cause internal short circuits, compromise cycling stability, and raise serious safety concerns. The main strategies for suppressing dendrite formation can be divided into five types: (i) the construction of artificial solid electrolyte interface[34-39], (ii) the incorporation of electrolyte additives[40-44], (iii) the structural design of Zn electrodes[45-49], (iv) the optimization of charging-discharging protocols[50-54], and (v) the use of solid or hydrogel electrolytes[55-59]. For example, a porous nano-$CaCO_3$ coating on a Zn electrode surface can guide Zn^{2+} deposition to occur evenly in the crevices among particles, enabling a 42.7% higher discharge capacity after 1,000 cycles than that of the bare Zn electrode (177 *vs*. 124 mAh g^{-1} at 1 A g^{-1})[60]. Additionally, a water-immiscible ionic liquid diluent can form a "water pocket" to suppress water activity, thereby mitigating the tip effect and reducing parasitic reactions[61]. When this additive was added to the electrolyte of the Zn-$Zn_{0.5}V_2O_5{\cdot}nH_2O$ battery, the battery could operate stably for 400 cycles at 60 °C, with a capacity retention greater than 85%. From a structural perspective, semiliquid Zn powder anodes mitigate plating-induced stress and increase the availability of active sites, supporting more than 5,000 stable cycles[49]. In addition, surface-structured Zn anodes homogenize Zn^{2+} flux by reducing the local current density and using the laminar flow of an etchant solution, which reflects the obvious synergistic effect between electrode surface structure design and electrolyte gradient engineering[62]. Furthermore, a current-controlled electrodeposition strategy has been shown to regulate the crystallographic orientation of Zn. Increasing the current density from 20 to 80 mA cm^{-2} induces a transition in the preferred growth plane from (101) to (002), with the (002) texture favouring more homogeneous Zn deposition[50,63]. Accordingly, full cells employing (002)-textured Zn anodes paired with V/Mn-based oxide cathodes exhibit improved cycling stability (Zn(002)-MnO_2 full cells have a reversible capacity of 206.1 mAh g^{-1} after 200 cycles with 0.2 A g^{-1}).

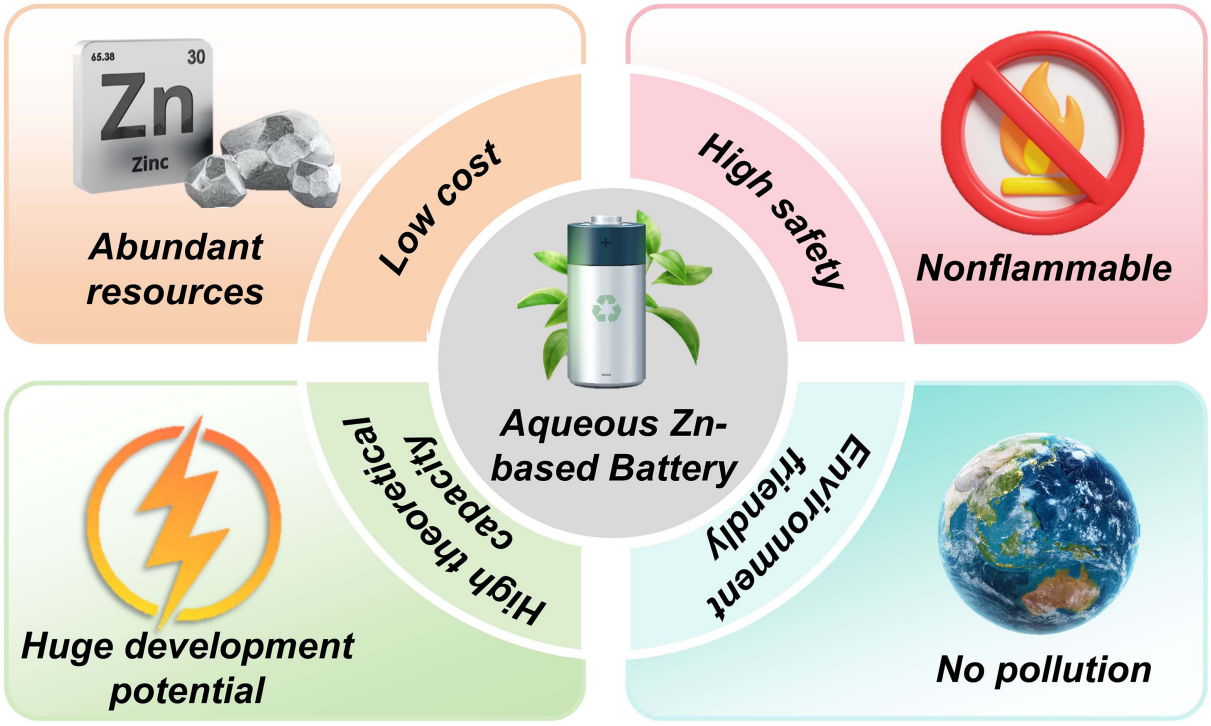

Figure 1. Advantages of aqueous Zn-based batteries.

Beyond the aforementioned Zn deposition regulation strategies, hydrogel electrolytes have emerged as effective platforms for stabilizing Zn plating/stripping behavior. Owing to their three-dimensional polymer networks, hydrogel electrolytes can simultaneously provide mechanical constraints and continuous ionic pathways, thereby reshaping the interfacial environment of Zn electrodes. For instance, multicrosslinked alkaline gel electrolytes demonstrate superior mechanical robustness and ionic conductivity, enabling batteries to operate stably under extreme conditions with high energy efficiency[64]. Beyond structural integrity, the molecular engineering of polymer side chains offers a precise means to dictate interfacial reactions. A notable example is the integration of heterocyclic tetrazole groups to create polymeric single-ion conductors, which achieve an exceptional Zn^{2+} transference number of 0.94 and significantly extend the shelf life of Zn batteries[65]. Furthermore, introducing high-valent cations such as Zr^{4+} into silk fibroin-based hydrogels not only reinforces the matrix but also guides epitaxial growth along the (002) plane, effectively suppressing parasitic side reactions even at high depths of discharge[66]. Collectively, these advancements underscore that the efficacy of interfacial strategies fundamentally hinges on "ion modulation". By sophisticatedly tailoring the local solvation structure and transport kinetics, these approaches converge on a central design principle: the construction and regulation of the ion concentration gradient.

To provide mechanistic insights into the stabilization of Zn electrode interfaces, this review systematically reviews state-of-the-art strategies for constructing Zn^{2+} concentration gradients in aqueous Zn-based batteries, covering both liquid electrolytes and solid-state hydrogel electrolytes. In liquid systems, Zn^{2+} concentration gradients are regulated through electrolyte chemistry, such as functional additives, and interfacial engineering approaches, including ion-selective separators, enabling the suppression of interfacial side reactions and the homogenization of ion flux[67]. In hydrogel systems, intrinsic ionic confinement within polymer networks introduces additional design flexibility, allowing gradient construction through tailored network architectures and spatially differentiated ionic environments[68]. By integrating these strategies, this review highlights that controlled Zn^{2+} concentration fields fundamentally govern ion transport pathways,

solvation and desolvation behavior, electric field distribution, and interfacial reaction kinetics. In this context, ion-concentration gradient engineering is distinguished from related concepts such as solvation structure regulation and general interfacial modification by treating the spatial distribution of Zn^{2+} as a primary and independent design parameter. While solvation regulation operates at the molecular scale and interfacial engineering focuses on surface stabilization, gradient engineering functions at the mesoscopic scale by deliberately constructing spatially nonuniform Zn^{2+} distributions, thereby establishing chemical potential gradients that directly regulate ion flux and deposition behavior. Importantly, solvation modulation and interfacial control can act as enabling mechanisms for gradient formation but do not inherently generate spatial asymmetry unless specifically designed. Therefore, ion-concentration gradient engineering represents an integrative framework that unifies transport regulation, solvation modulation, and interfacial control under the concept of spatially resolved ion distribution, providing a coherent theoretical basis for understanding and designing stable and high-performance aqueous Zn batteries.

GRADIENT ENGINEERING IN LIQUID ELECTROLYTES

In liquid electrolyte systems, concentration gradient engineering serves as a fundamental strategy for regulating Zn^{2+} transport and interfacial reactions, thereby stabilizing Zn electrode behavior. Owing to the high mobility of ions and solvent molecules, liquid electrolytes are particularly sensitive to local concentration fluctuations and interfacial chemistry. By deliberately introducing spatially asymmetric ion distributions, it becomes possible to modulate the Zn^{2+} solvation structure, electric double-layer configuration, and ion flux near the electrode surface. In this regard, various approaches have been developed to construct ion concentration gradients in liquid electrolytes, primarily through the use of functional electrolyte additives and ion-selective separators.

Functional additive regulation

In conventional aqueous liquid electrolytes, functional additives enable the construction of Zn^{2+} concentration gradients primarily through competitive coordination, interfacial adsorption, and modulation of the electric double layer. Additives containing electron-donating functional groups can partially replace water molecules in the primary solvation sheath of Zn^{2+}, thereby reconstructing its solvation structure and altering desolvation kinetics[69,70]. Owing to their preferential adsorption on the Zn surface, these additives locally increase the amount of coordinated Zn^{2+} ions at the electrode and electrolyte interface, generating spatial asymmetry in the chemical potential between the bulk electrolyte and the interfacial region. This gradient drives directional Zn^{2+} flux, alleviates ion depletion during plating, and homogenizes nucleation behavior, thereby suppressing dendrite growth and stabilizing interfacial reactions.

On the basis of this mechanism, Wang *et al.* introduced N, S-doped quantum dots (NSQDs) into the electrolyte to construct a surface Zn^{2+} concentration gradient and regulate deposition behavior[71]. The mechanistic basis lies in the abundance of oxygen-containing functional groups located on the side chains of the NSQDs. Upon contact with the Zn foil, these groups undergo partial reduction and anchor onto the metal surface, forming Zn-O bonds[72]. This interfacial chemical coupling creates a Zn^{2+}-affinitive layer that is locally enriched with Zn^{2+} ions near the electrode, generating a directional ion flux from the bulk electrolyte toward the surface. As a result, numerous uniformly distributed nucleation sites are established, lowering the nucleation overpotential and homogenizing Zn electrodeposition[73]. The formation of this functional interfacial layer was verified by energy dispersive X-ray spectroscopy (EDS) mapping, which revealed uniform distributions of O, N, and S, which were consistent with those of the NSQDs coating, confirming intimate interfacial integration [Figure 2A]. Owing to the regulated Zn^{2+} distribution, the Zn electrode exhibited a significantly smoother and denser morphology after 10 cycles in a symmetric cell at 10 mA cm^{-2} with an areal capacity of 0.5 mAh cm^{-2}, as evidenced by scanning electron microscopy (SEM) [Figure 2B]. This interfacial gradient effect is further translated into remarkable full-cell performance. In a Zn-zinc

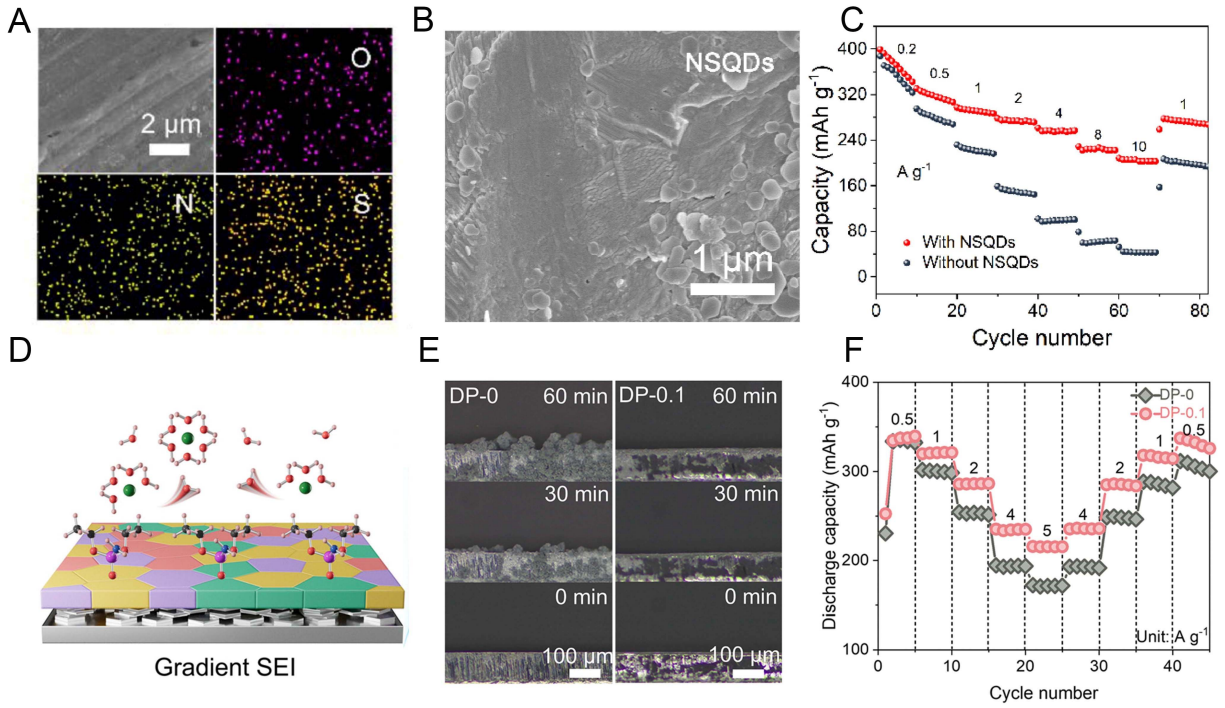

Figure 2. (A) SEM image and corresponding EDS mapping of the Zn electrode, which is soaked with the NSQDs dispersion[71]. (B) SEM image after 10 cycles at 10 mA cm^{-2} and 0.5 mAh cm^{-2} with the NSQDs additive[71]. (C) Rate performance comparison of Zn-ZVO with and without NSQDs[71]. (A-C) Reproduced with permission from[71]. Copyright 2023, Elsevier. (D) Schematic illustration of the DP additive effect at the electrode/electrolyte interface[77]. (E) Operando optical microscopy images of Zn deposition in DP-0 and DP-0.1 electrolytes at 5 mA cm^{-2}[77]. (F) Rate capability of Zn||NVO full cells with DP-0 and DP-0.1 electrolytes[77]. (D-F) Reproduced with permission from[77]. Copyright 2025, Royal Society of Chemistry.

vanadate (ZVO) configuration, the NSQDs-modified system maintained a high specific capacity of 208.4 mAh g^{-1} even at an ultrahigh current density of 10 A g^{-1}, substantially outperforming its conventional electrolyte counterpart (44.4 mAh g^{-1}). When the current density was restored to 1 A g^{-1}, the cell recovered a high capacity of 278.9 mAh g^{-1}, demonstrating excellent rate capability and reversibility [Figure 2C]. These improvements originate from additive-induced interfacial Zn^{2+} enrichment and the resulting mitigation of localized ion depletion, which collectively suppress dendrite growth and stabilize the electrochemical reaction environment.

Additive hydrogen bond interactions offer an effective strategy to regulate the Zn electrode interface by restructuring the interfacial water network and tuning Zn^{2+} solvation chemistry. In aqueous electrolytes, the hydrogen-bonded network of water governs proton activity, Zn^{2+} coordination structure, and interfacial reaction kinetics[74]. The introduction of hydrogen bond-active additives, such as molecules containing hydroxyl, amino, or carbonyl functional groups, enables competitive interactions with water molecules, thereby reducing free water activity and weakening proton transport pathways[75,76]. This suppression of interfacial water reactivity mitigates the hydrogen evolution reaction and limits the formation of hydroxide byproducts. Simultaneously, the adsorption and interfacial enrichment of such additives reconstruct the electric double layer and modify the Zn^{2+} solvation sheath, lowering the desolvation barriers and homogenizing the ion flux. The resulting asymmetric hydrogen-bond environment establishes an ordered interfacial microstructure, which alleviates local ion depletion, stabilizes Zn nucleation, and improves deposition uniformity.

On the basis of this mechanism, Zong *et al.* introduced diethyl phosphoramidate (DP) as an electrolyte additive to simultaneously regulate hydrogen bonding interactions and Zn^{2+} solvation behavior[77]. The polar

P=O and N-H functional groups in DP strongly interact with water molecules, disrupting the intrinsic hydrogen bonding network of the aqueous electrolyte and thereby reducing free water activity[78]. This suppression of water reactivity mitigates interfacial pH fluctuations and inhibits parasitic side reactions, particularly the hydrogen evolution reaction. Moreover, DP participates in the Zn^{2+} solvation sheath, partially replacing coordinated water molecules and reconstructing the local coordination environment[79]. The modified solvation structure decreases the desolvation energy barrier and accelerates interfacial charge transfer kinetics while simultaneously decreasing the probability of water reduction at the electrode surface. Beyond solvation regulation, DP undergoes interfacial reactions that generate a gradient organic-inorganic hybrid solid electrolyte interphase (SEI) *in situ* [Figure 2D]. This interphase, enriched with DP-derived species and inorganic Zn compounds, provides abundant and energetically favourable nucleation sites, guiding Zn deposition preferentially along the thermodynamically stable (002) crystallographic plane. The resulting interfacial layer not only homogenizes the electric field distribution but also establishes a more uniform Zn^{2+} flux toward the electrode surface, thereby suppressing dendrite formation[43]. *In situ* optical observations at 5 mA cm^{-2} clearly reveal this regulatory effect. In the absence of DP, Zn deposition rapidly develops surface protrusions that evolve into dendritic structures, and this behavior indicates severe ion flux heterogeneity. In contrast, the DP-containing electrolyte enables dense and uniform Zn plating throughout the deposition process, and these results confirm that the reconstructed interfacial microenvironment promotes homogeneous nucleation and growth [Figure 2E]. The interfacial stabilization induced by DP translates directly into enhanced electrochemical performance at the full-cell level. Although cells with and without DP exhibit comparable initial capacities at low current density, the DP-modified system maintains a substantially higher capacity under high-rate conditions and demonstrates excellent reversibility upon returning to lower current densities [Figure 2F]. These improvements originate from the synergistic effects of hydrogen bond disruption, solvation-structure reconstruction, and gradient SEI formation, which collectively alleviate interfacial side reactions, homogenize Zn^{2+} distribution, and stabilize long-term Zn plating/stripping behavior.

Ion-selective separator regulation

In conventional liquid electrolyte systems, ion concentration gradients can be deliberately constructed by introducing functional separators with selective ion transport properties between the anode and cathode. Unlike inert porous membranes that serve only as physical barriers, these engineered separators contain fixed charges, polar functional groups, or well-defined ion-conductive channels that regulate Zn^{2+} migration through electrostatic interactions, selective coordination, and Donnan exclusion effects[80,81]. This selective transport behavior redistributes Zn^{2+} flux and creates spatial asymmetry in the ion concentration within the electrolyte region, thereby establishing a controlled chemical potential gradient toward the Zn electrode surface. Moreover, the tailored internal structure of the separator modulates the local electric field distribution and constrains ion diffusion pathways, which alleviates localized ion depletion and suppresses the field amplification that typically drives dendritic growth. In certain systems, solvent transport and water activity near the anode are also regulated, leading to reduced hydrogen evolution and surface passivation. Through the combined effects of ion sieving, electric field homogenization, and mass transport control, functional separators provide an effective platform for stabilizing Zn^{2+} flux and improving interfacial deposition behavior.

On the basis of this design principle, Liu *et al.* developed a bifunctional composite separator (BC-FP) using a nanoconfinement and gradient ion-guiding strategy to regulate Zn^{2+} transport and deposition[82]. The separator integrates a bacterial cellulose layer with a filter paper substrate, enabling synergistic control over ion migration and interfacial kinetics. The bacterial cellulose component is rich in zincophilic hydroxyl groups that can coordinate with Zn^{2+} ions, thereby reconstructing local transport pathways and stabilizing the interfacial microenvironment by suppressing parasitic side reactions [Figure 3A]. Moreover, the

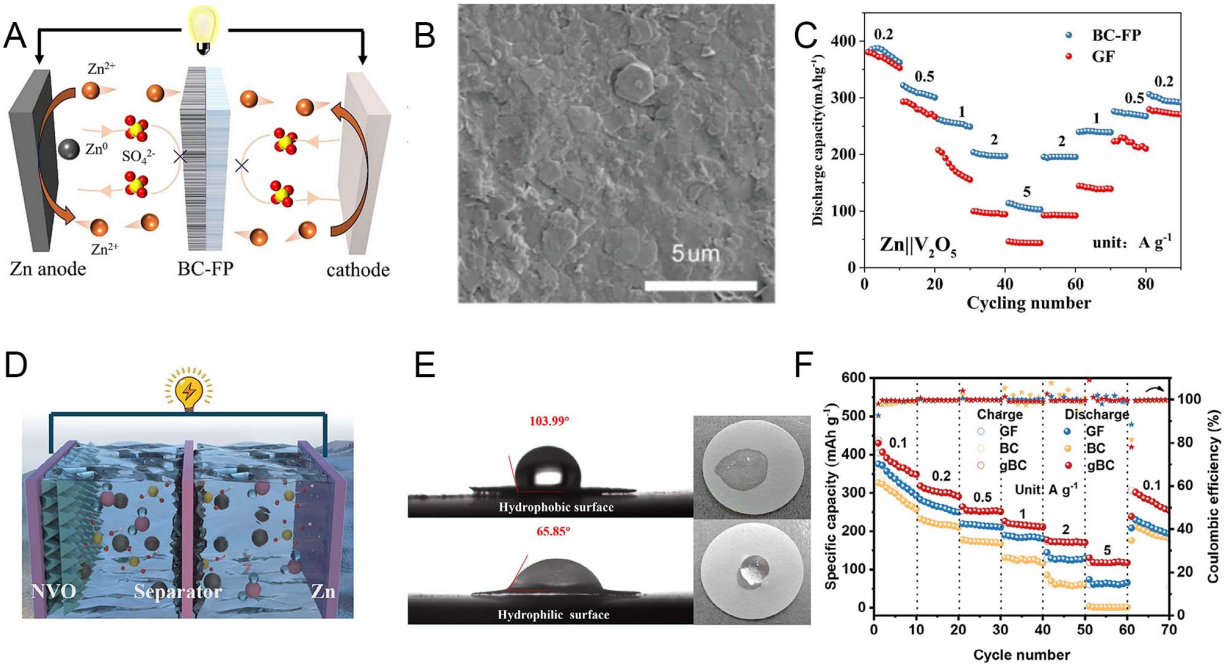

Figure 3. (A) Schematic illustration of the assembled Zn-V_2O_5 full cell with a 2 M $ZnSO_4$ electrolyte[82]. (B) SEM image of Zn electrodes after 30 min of cycling at 1 mA cm^{-2} with a BC-FP separator[82]. (C) Rate performance of Zn-V_2O_5 full cells with BC-FP and GF separators from 0.2 to 5 A g^{-1}[82]. (A-C) Reproduced with permission from[82]. Copyright 2025, Elsevier. (D) Schematic illustration of the Zn-NVO full-cell working mechanism[85]. (E) Contact angle of the gBC separator with corresponding optical images[85]. (F) Rate performance of Zn-NVO full cells with GF, BC, and gBC separators[85]. (D-F) Reproduced with permission from[85]. Copyright 2026, Wiley-VCH GmbH.

hydrophilic filter paper layer facilitates directional Zn^{2+} transport through capillary-driven electrolyte uptake, promoting a continuous and guided ion flux toward the anode. The intrinsic gradient pore structure across the composite further modulates mass transport by enhancing ion diffusion while preventing localized ion depletion. This structural asymmetry establishes a spatially regulated Zn^{2+} concentration profile and homogenizes the desolvation process of hydrated Zn^{2+} ions at the electrode surface, leading to uniform nucleation behavior. After cycling a Zn symmetric cell at 1 mA cm^{-2} for 30 min, the Zn electrode under BC-FP conditions exhibited a dense and smooth surface morphology, indicating that the Zn deposition stabilized compared with that of conventional separators [Figure 3B]. In full cells employing a Zn anode and a vanadium-based cathode, the BC-FP separator consistently delivers higher specific capacities across a wide range of current densities than glass fibre separators do. At high rates, the capacity advantage becomes particularly pronounced, and the cell maintains excellent reversibility when the current density is restored to lower values [Figure 3C].

In addition to directly regulating ion transport, ion concentration gradients can also be engineered by tailoring the interactions between separators and water molecules, thereby indirectly modulating Zn^{2+} solvation and interfacial mass transport. In aqueous electrolytes, water not only serves as the solvent but also governs proton activity, hydrogen bonding networks, and the solvation structure of Zn^{2+} ions. By introducing separators with strong water affinity, hydrogen bond acceptor or donor groups, or confined hydrophilic nanochannels, the local distribution and mobility of water molecules can be spatially regulated. Such separators can preferentially adsorb or immobilize water within their matrix, effectively reducing free water activity near the Zn electrode and reconstructing the hydrogen bonding network[83,84]. This confinement alters the primary solvation sheath of Zn^{2+}, often decreasing the number of coordinated water molecules and lowering desolvation barriers at the interface. Simultaneously, the asymmetric distribution of water across the separator establishes a gradient in solvent activity and chemical potential, which indirectly drives a more

uniform Zn^{2+} flux toward the electrode surface. This regulated interfacial microenvironment mitigates pH fluctuations, suppresses hydrogen evolution, and prevents the accumulation of hydroxide byproducts.

On the basis of this mechanism, Dong *et al.* developed an 18 μm thick cellulose separator with a negatively charged surface and gradient hydrophobicity to regulate the solvent distribution and Zn^{2+} transport[85]. The negatively charged functional groups within the separator create an electrostatic shielding effect that repels Cl^- anions while promoting more uniform Zn^{2+} flux through selective ion migration [Figure 3D]. Moreover, the gradient hydrophobic architecture induces asymmetric wettability across the separator thickness, as evidenced by the distinct water contact angles on the two surfaces, which confirms the establishment of a spatially differentiated solvent environment [Figure 3E]. This asymmetric solvent distribution results in a stepwise desolvation pathway for hydrated Zn^{2+} ions, gradually reducing the number of coordinated water molecules as the ions approach the anode. The resulting localized high-concentration electrolyte environment near the electrode effectively suppresses hydrogen evolution and mitigates interfacial side reactions. Through the combined effects of electrostatic regulation, solvent confinement, and progressive desolvation, the separator homogenizes interfacial Zn^{2+} transport and stabilizes deposition behavior. Consequently, compared with control systems lacking gradient structural design, full cells employing this separator exhibit superior rate capability and consistently higher specific capacities across a wide range of current densities, demonstrating that solvent-mediated gradient engineering is an effective strategy for enhancing the interfacial stability and electrochemical performance of AZBs [Figure 3F].

Notably, the formation of ion concentration gradients is not merely a secondary consequence of interfacial modification but also serves as a fundamental driving factor governing Zn deposition behavior. While interfacial phenomena such as solid electrolyte interphase formation, surface adsorption, and solvation structure regulation can influence local electrochemical environments, their primary role in many systems is to induce or stabilize spatially nonuniform Zn^{2+} distributions. These gradients establish chemical potential differences that directly regulate the ion flux, electric field distribution, and nucleation kinetics at the Zn electrode surface. In this sense, ion concentration gradients represent the underlying physical origin of homogenized Zn^{2+} transport and uniform deposition.

Moreover, it is important to recognize that gradient formation is often intrinsically coupled with other interfacial effects. For example, additive adsorption or SEI formation can simultaneously modify the electric double layer and promote localized Zn^{2+} enrichment, while confined polymer networks in hydrogel systems regulate both ion transport and solvent activity[86]. These processes act cooperatively to reinforce gradient stability and amplify its regulatory effect on interfacial reactions. Therefore, rather than being independent or competing mechanisms, ion concentration gradients and interfacial modifications should be understood as synergistically coupled, where gradients provide the primary driving force for Zn^{2+} flux regulation, and interfacial effects serve as essential enablers that facilitate and stabilize the gradient structure.

GRADIENT ENGINEERING IN HYDROGEL ELECTROLYTES

In hydrogel electrolyte systems, concentration gradient engineering offers a versatile and effective pathway for regulating ion transport and stabilizing the Zn electrode interface. Owing to their intrinsic polymer networks and tunable physicochemical properties, hydrogel electrolytes enable spatially resolved control over ion migration, solvation structure, and interfacial water activity, which is difficult to achieve in conventional liquid electrolytes[87,88]. By rationally designing heterogeneous or asymmetric hydrogel architectures, it becomes possible to construct regulated Zn^{2+} concentration fields across the electrolyte, thereby guiding ion flux and interfacial reactions. In this context, various gradient construction strategies, such as network density modulation, functional group distribution, compositional layering, and additive-assisted regulation, have been developed to exploit the unique ion transport behavior of hydrogels.

It should be clarified that gradient structures are fundamentally distinct from general structural heterogeneity. While heterogeneity refers to irregular or nonuniform distributions of network features without defined spatial control, gradient design involves continuous and directional variation in structure or composition, leading to spatially resolved differences in Zn^{2+} concentration[89]. This directional asymmetry establishes a chemical potential gradient that actively guides Zn^{2+} transport and regulates ion flux at the electrode interface. Therefore, the key distinction lies in the ability of gradient structures to impose controlled ion transport pathways rather than merely introducing structural nonuniformity.

Gradient network architecture

By designing distinct network structures in different regions of hydrogel electrolytes, ion concentration gradients can be established through spatially differentiated ion transport and solvent confinement behavior. In hydrogel systems, the polymer network governs ion mobility, water distribution, and Zn^{2+} solvation structure by controlling pore size, crosslinking density, and the distribution of functional groups. Regions with high crosslinking density or reduced pore size impose stronger confinement effects, lowering ion diffusivity and partially immobilizing water molecules, whereas loosely crosslinked domains provide faster ion migration pathways and higher ionic conductivity. This structural heterogeneity generates differences in Zn^{2+} transport kinetics and local chemical potential across the hydrogel, thereby creating a controllable ion concentration gradient[89,90]. Simultaneously, functional groups embedded within the polymer matrix can selectively coordinate with Zn^{2+} or participate in hydrogen bonding with water, further modulating the solvation structure and desolvation dynamics near the electrode interface. As hydrated Zn^{2+} ions migrate from bulk-like regions toward more confined domains adjacent to the anode, a progressive desolvation process occurs, leading to localized Zn^{2+} enrichment and reduced water activity at the interface. This asymmetric microenvironment homogenizes the ion flux, suppresses hydrogen evolution, and stabilizes Zn nucleation behavior.

On the basis of this principle, Wang *et al.* developed a gradient network hydrogel electrolyte composed of polyvinyl alcohol (PVA), cellulose nanofibres (CNF), and graphene oxide (GO) to regulate Zn^{2+} transport and interfacial kinetics in AZBs[91]. The design integrates a low-density PVA and CNF (PC) layer on the cathode side with a high-density PVA, CNF, and GO (PCG) layer adjacent to the Zn anode, thereby establishing spatially differentiated transport properties within a single electrolyte. The cathode-facing layer contains wider transport channels and a higher water content, which facilitates rapid ion migration and maintains high ionic conductivity [Figure 4A]. In contrast, the dense interfacial network enriched with carboxyl and hydroxyl groups enhances Zn^{2+} coordination and promotes progressive desolvation as ions approach the anode. This confined microenvironment reduces local water activity, suppresses parasitic reactions, and homogenizes Zn^{2+} flux at the electrode surface. Simulated Zn^{2+} concentration fields confirm that compared with homogeneous hydrogels, the gradient structure results in a more uniform interfacial ion distribution, which is consistent with the proposed mechanism of concentration gradient regulation. The electrochemical benefits are reflected in the rate performance, where cells employing the gradient hydrogel deliver average discharge capacities of 250.6, 236.2, 205.7, 159.3, 125.0, 103.6, 89.7, and 236.5 mAh g^{-1} at current densities of 0.15, 0.3, 0.6, 1.2, 1.8, 2.4, 3, and 0.15 A g^{-1}, respectively [Figure 4B]. These values consistently exceed those obtained with hydrogels with homogeneous structures, demonstrating that gradient network engineering effectively regulates Zn^{2+} transport, stabilizes interfacial deposition, and enhances overall electrochemical performance.

Gradient concentration fields can also be constructed through the formation of chemical bonds between the hydrogel electrolytes and the Zn electrode surface, which creates an interfacially anchored and chemically coupled transport layer. When functional groups within the hydrogel network, such as hydroxyl, carboxyl, amino, or sulfonate groups, form coordination or covalent interactions with surface Zn atoms, a tightly

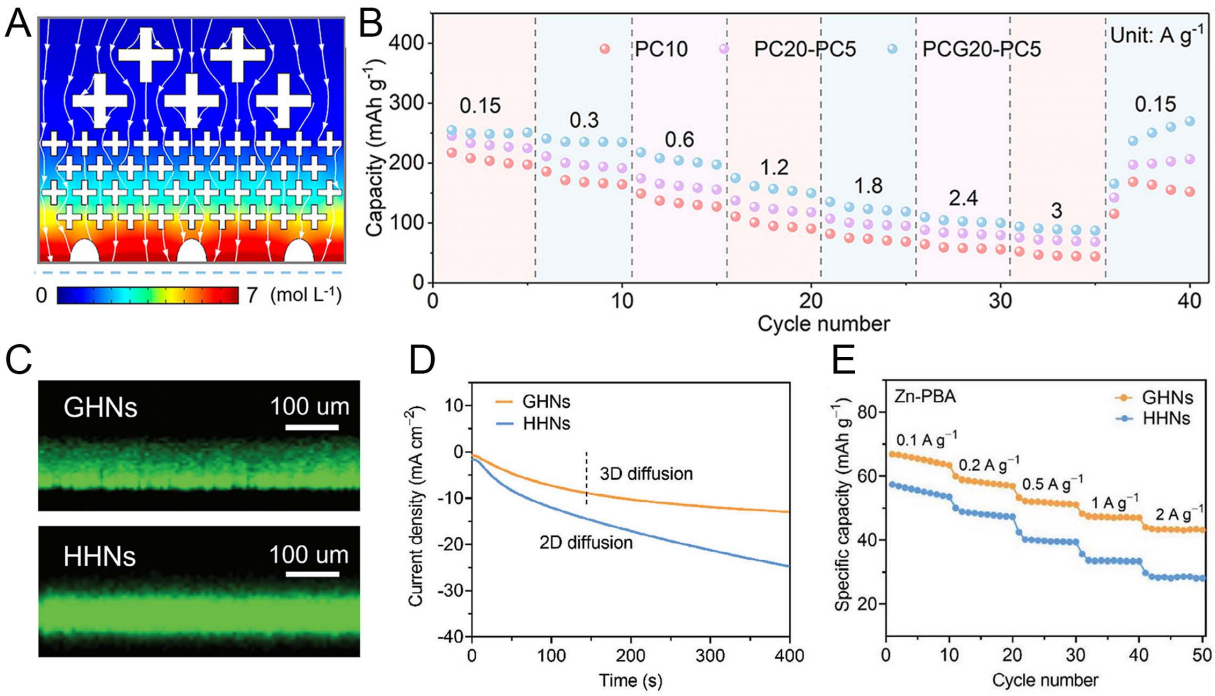

Figure 4. (A) Simulated ionic field distributions in PCG20-PC5 systems based on schematic models[91]. (B) Rate performance of Zn-MnO_2 full cells[91]. (A and B) Reproduced with permission from[91]. Copyright 2025, American Chemical Society. (C) CLSM visualization of the GHNs and HHNs[90]. (D) Chronoamperometry of Zn metal in the GHNs and HHNs at -150 mV overpotential[90]. (E) Rate capabilities of Zn-GHNs-PBA and Zn-HHNs-PBA at 0.1-2 A g^{-1} within a 1-2 V operating window[90]. (C-E) Reproduced with permission from[90]. Copyright 2024, Wiley-VCH GmbH.

bound interphase is generated that differs structurally and chemically from the bulk gel[57,92]. Compared with the interior hydrogel matrix, this bonded interfacial region exhibits modified ion mobility, solvent distribution, and coordination environments. Chemical anchoring enhances Zn^{2+} affinity at the interface and promotes localized ion enrichment, thereby establishing a spatial gradient in Zn^{2+} concentration from the bulk electrolyte toward the electrode surface. Simultaneously, the constrained polymer chains and coordinated functional groups facilitate partial desolvation of hydrated Zn^{2+} ions and reduce free water activity in the interfacial zone, which suppresses hydrogen evolution and mitigates surface passivation. Interfacial bonding also stabilizes the electric field distribution and minimizes interfacial impedance fluctuations during repeated plating and stripping. Through the synergistic effects of chemical anchoring, solvation reconstruction, and mass transport modulation, hydrogel-Zn interfacial bonding provides a robust strategy for generating controlled concentration gradients and enhancing Zn deposition uniformity and cycling stability in AZBs.

On the basis of this concept, Cui *et al.* constructed gradient hydrogel networks via an epitaxial polymerization strategy that enables covalent anchoring of the polymer matrix onto the Zn surface[90]. The resulting networks exhibit an asymmetric distribution of negatively charged groups along the thickness direction, which promotes selective Zn^{2+} transport and increases the Zn^{2+} transference number to 0.65, markedly higher than that of homogeneous hydrogel networks with identical polymer contents. Confocal laser scanning microscopy (CLSM) revealed that the network density gradually decreased from the Zn side interface toward the bulk region, confirming the well-defined gradient architecture, whereas homogeneous hydrogels displayed uniform density along the Z axis [Figure 4C]. This structural asymmetry establishes differentiated ion mobility and solvent confinement, where the dense interfacial layer restricts lateral diffusion and regulates Zn^{2+} desolvation, while the upper region maintains sufficient ionic conductivity. Chronoamperometric measurements further elucidate the transport mechanism. In homogeneous hydrogels,

the continuously increasing current within 400 s indicates two-dimensional diffusion and nonuniform deposition [Figure 4D]. In contrast, the gradient hydrogel exhibited a stable current plateau after 143 s, characteristic of three-dimensional diffusion, demonstrating that the high-density interfacial network effectively homogenized the Zn^{2+} flux and stabilized the nucleation behavior[82]. Notably, the term "stable" used here does not imply a strictly constant current response but rather refers to the relatively reduced fluctuation amplitude and smoother evolution of the current over time. These interfacial transport advantages translate to improved electrochemical performance, with full cells delivering capacities of 67, 60, 53, 48, and 44 mAh g^{-1} at current densities of 0.1, 0.2, 0.5, 1, and 2 A g^{-1}, respectively, compared with 57, 50, 43, 36, and 30 mAh g^{-1} for homogeneous hydrogel systems [Figure 4E]. The superior rate capability confirms that covalently anchored gradient networks effectively regulate interfacial ion transport and reaction kinetics at the Zn electrode.

Asymmetric multilayer designs

Hydrogel electrolytes possess sufficient mechanical robustness and structural flexibility to enable the lamination of multiple hydrogel layers with distinct physicochemical properties, thereby providing a platform for constructing spatially controlled ion concentration gradients. When hydrogels with different crosslinking densities, pore structures, functional group distributions, or water contents are stacked together, each layer exhibits unique ion transport kinetics, solvent activity, and Zn^{2+} coordination behavior. Regions with loose networks and high water content typically offer high ionic conductivity and rapid Zn^{2+} migration, whereas densely crosslinked or functionally enriched layers impose stronger confinement effects, reduce water mobility, and enhance Zn^{2+} coordination interactions[93,94]. This structural heterogeneity generates differences in diffusion coefficients and chemical potentials across the electrolyte thickness, resulting in a directional Zn^{2+} flux from high-mobility domains toward more confined interfacial regions. As hydrated Zn^{2+} ions traverse these layers, progressive desolvation and solvent reorganization occur, leading to localized Zn^{2+} enrichment and reduced free water activity near the electrode surface. The resulting asymmetric transport environment homogenizes the interfacial ion distribution, suppresses hydrogen evolution, and stabilizes Zn nucleation and growth. Through the integration of mass transport modulation, solvent confinement, and solvation structure tuning, laminated hydrogel electrolytes enable rational gradient engineering to enhance the interfacial stability and electrochemical performance of AZBs.

On the basis of this concept, Lu *et al.* proposed a directional electrolyte gradient strategy that establishes a Zn^{2+} concentration gradient from the separator toward the anode to simultaneously optimize wettability and interfacial deposition behavior[95]. In this configuration, a high-concentration electrolyte integrated with a sodium carboxymethyl cellulose binder is coated directly onto the Zn surface, while a low-concentration electrolyte fully infiltrates the glass fibre separator [Figure 5A]. This spatially differentiated design creates distinct physicochemical environments across the cell. The low-concentration region ensures sufficient wettability and facilitates long-range Zn^{2+} migration within the separator, whereas the high-concentration region adjacent to the Zn anode promotes dense and uniform Zn deposition by reducing water activity, suppressing parasitic reactions, and stabilizing the interfacial electric field. Optical observations after 10 h of evaporation reveal a gradual transition in light transmittance from top to bottom, which is consistent with an increasing concentration of crystalline hydrated zinc sulfate, confirming the formation of the intended concentration gradient [Figure 5B]. The distribution of carboxymethyl cellulose particles further supports this gradient structure, with spherical and chain-like aggregates concentrated near the bottom region and flake-like structures observed near the top, reflecting morphology-dependent migration behavior during solvent redistribution. The electrochemical advantages of this gradient design are evident in full cells assembled with Zn anodes and V_2O_5 cathodes. Under gradient electrolyte conditions, the cell retains a specific capacity of 92 mAh g^{-1} after 800 cycles, whereas a cell using a conventional liquid electrolyte decreases to 37 mAh g^{-1} after only 200 cycles. The gradient system also exhibits more stable and narrowly

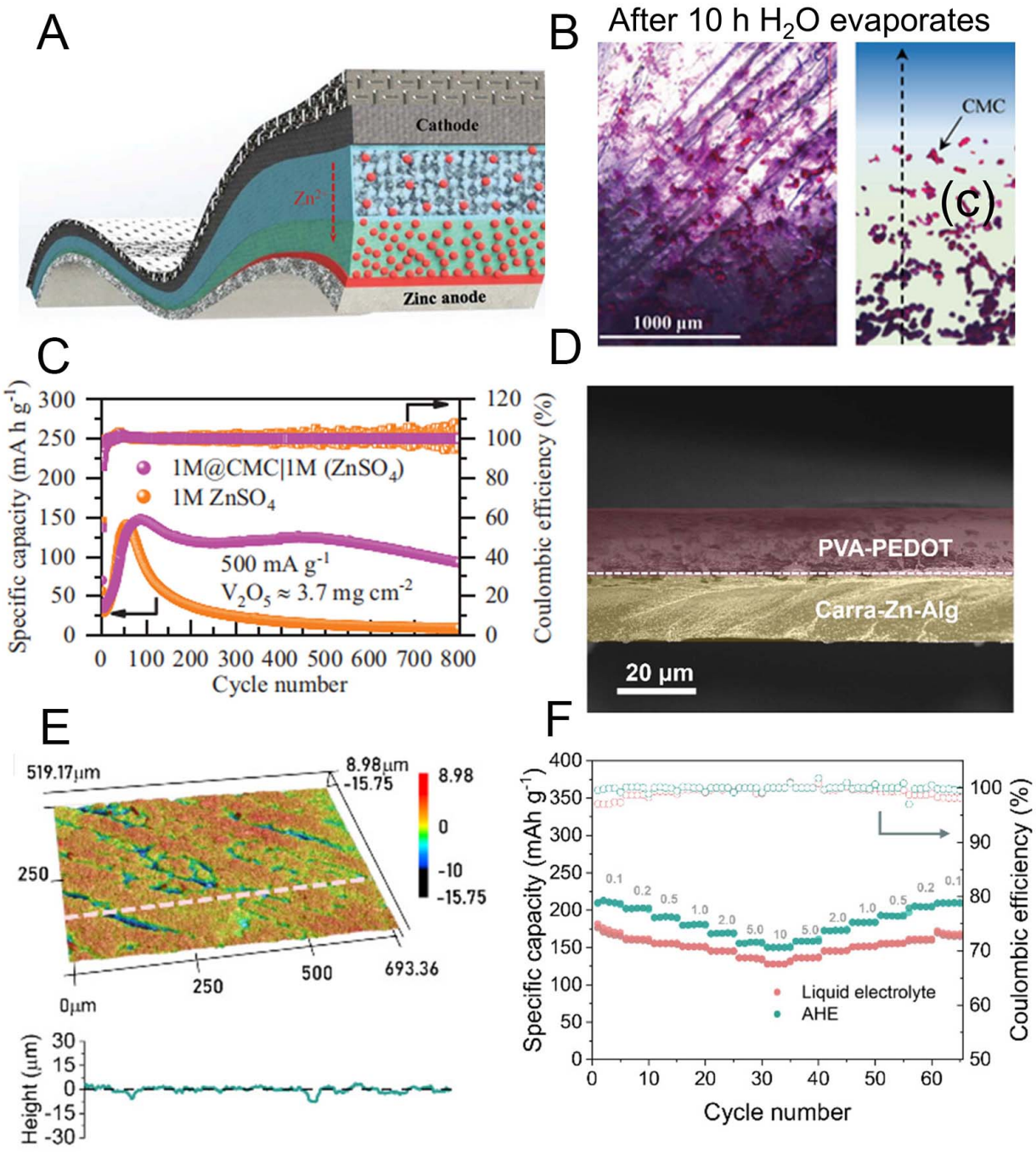

Figure 5. (A) Schematic of the gradient electrolyte strategy for AZBs[95]. (B) Optical photograph showing the concentration distribution of CMC in the gradient electrolyte[95]. (C) Discharge capacity and Coulombic efficiency of Zn-V_2O_5 cells with 1 M $ZnSO_4$ and 1 M@CMC|1 M $ZnSO_4$ electrolytes at 500 mA g^{-1}[95]. (A-C) Reproduced with permission from[95]. Copyright 2023, Wiley-VCH GmbH. (D) Cross-section of the AHE[96]. (E) CLSM image of the Zn anode after 100 h in the hydrogel electrolyte[96]. (F) Zn-I_2 full-cell rate performance from 0.1 to 10 A g^{-1}[96]. (D-F) Reproduced with permission from[96]. Copyright 2024, American Chemical Society.

distributed Coulombic efficiency, indicating suppressed side reactions and stabilized interfacial kinetics [Figure 5C]. These results demonstrate that a spatially controlled electrolyte concentration effectively regulates Zn^{2+} flux and interfacial reactions, leading to significantly enhanced cycling stability.

Moreover, this gradient electrolyte design strategy can be extended to Zn-I_2 battery systems, where it simultaneously regulates Zn anode stability and iodine redox kinetics through spatially differentiated ionic

environments. In Zn-I_2 batteries, performance degradation typically arises from two coupled issues: dendritic Zn deposition at the anode and the dissolution and shuttling of polyiodide species at the cathode[96]. By constructing a Zn^{2+} concentration gradient from the separator toward the Zn surface, a high-concentration electrolyte region adjacent to the anode reduces water activity, suppresses hydrogen evolution, and homogenizes Zn^{2+} flux, thereby stabilizing Zn plating and stripping. Moreover, maintaining a relatively low concentration environment near the separator and cathode preserves sufficient ionic conductivity and facilitates efficient redox conversion of iodine species[97,98]. Concentration asymmetry also influences the distribution and diffusion behavior of polyiodide intermediates, as modified solvent activity and ion-pairing interactions can restrict their outwards migration and mitigate shuttle effects. Consequently, the gradient electrolyte establishes a coordinated regulatory mechanism that balances Zn^{2+} transport, solvent reactivity, and iodine conversion dynamics.

On the basis of this principle, Liu *et al.* constructed an asymmetric hydrogel electrolyte to achieve spatially differentiated interfacial regulation in Zn-I_2 batteries[96]. On the anode side, a Zn^{2+}-crosslinked sodium alginate and carrageenan double-network hydrogel was employed to guide Zn^{2+} transport and stabilize the deposition behavior [Figure 5D]. The abundant coordination sites within this dense network promote uniform Zn^{2+} distribution, facilitate controlled desolvation, and suppress dendritic growth, thereby enabling dendrite-free Zn plating and long-term interfacial stability. On the cathode side, a highly conductive PVA-reinforced poly(3,4-ethylenedioxythiophene) polystyrene hydrogel (PVA-PEDOT) was introduced to immobilize polyiodide intermediates and accelerate electron transfer, effectively mitigating the shuttle effect while enhancing I_2 to I^- redox kinetics. This asymmetric configuration integrates ion transport regulation at the anode with redox confinement at the cathode, forming a coordinated gradient microenvironment across the cell. After operation at 5 mA cm^{-2} for 100 h, the Zn surface remained flat and dense, with a height variation of only 24 μm, confirming highly uniform deposition [Figure 5E]. The electrochemical advantages are reflected in the rate performance, where the full cell delivers capacities of 210 and 150 mAh g^{-1} at 0.1 and 10 A g^{-1}, respectively, and nearly fully recovers its initial capacity when the current density returns to 0.1 A g^{-1} [Figure 5F]. Compared with cells using conventional liquid electrolytes, cells using asymmetric hydrogel electrolytes demonstrate markedly improved stability and reversibility, highlighting the effectiveness of spatially engineered hydrogel systems in regulating interfacial reactions and enhancing battery performance.

Additive-assisted designs

Like conventional liquid systems, ion concentration gradients in hydrogel electrolytes can be established through the incorporation of functional additives that synergistically interact with both the polymer network and solvated Zn^{2+} species. In hydrogel matrices, ion transport is inherently influenced by network confinement, fixed charges, and solvent distribution. When additives containing coordination groups or hydrogen bond-active moieties are introduced, they can selectively bind Zn^{2+} ions or restructure the local water environment, thereby modifying solvation configurations and ion mobility within specific regions of the gel. Because diffusion and segmental motion in hydrogels are spatially heterogeneous, compared with those in additive-free regions, Zn^{2+} transport kinetics and chemical potentials in hydrogels in additive-enriched regions often differ[58,99]. This spatial variation generates a controllable Zn^{2+} concentration gradient across the electrolyte thickness. Near the anode interface, additive-induced coordination and solvent confinement promote progressive desolvation, reduce free water activity, and homogenize Zn^{2+} flux, whereas the bulk region maintains sufficient ionic conductivity for efficient charge transport. In some systems, additive participation in interfacial reactions further stabilizes the electrode surface by forming a reinforced interphase integrated with the polymer network. Through the combined effects of solvation tuning, selective coordination, and network-dependent mass transport modulation, additive functionalization in hydrogel electrolytes provides a versatile strategy for constructing ion concentration gradients and enhancing interfacial stability in AZBs.

On the basis of this strategy, Liu *et al.* introduced a zincophilic betaine (BT) additive into a functional hydrogel electrolyte to regulate interfacial chemistry and construct a favourable solid electrolyte interphase[100]. Owing to the robust interfacial contact established by the *in situ* sol-gel transition, BT molecules preferentially adsorb onto the Zn surface through their zinc-affinitive -COO groups, whereas the hydrophobic -CH_3 groups orient toward the electrolyte, thereby reconstructing the electric double layer and inducing the formation of a hybrid SEI with an organic-rich outer layer [Figure 6A]. This adsorption configuration displaces water molecules from the inner Helmholtz plane and simultaneously suppresses their replenishment from the outer Helmholtz plane, establishing a water-deficient interface that mitigates hydrogen evolution and other parasitic reactions. Compared with its *ex situ*-assembled counterpart, the *in situ*-constructed Zn/gel-BT/Zn symmetric cell exhibits markedly lower interfacial resistance, confirming improved interfacial contact and accelerated Zn^{2+} transport [Figure 6B]. Owing to the regulated SEI formation and homogenized ion flux, the symmetric cell achieves stable cycling for up to 450 h at 5 mA cm^{-2} and 10 mAh cm^{-2} [Figure 6C]. In Zn-Cu asymmetric cells, the gel BT electrolyte maintains exceptionally high Coulombic efficiency as the current density increases from 1 to 10 mA cm^{-2} and preserves ultrahigh reversibility when the current density is switched back to 1 mA cm^{-2}, whereas cells without BT display pronounced efficiency fluctuations under elevated current densities [Figure 6D]. These results collectively demonstrate that BT-enabled interfacial reconstruction in hydrogel electrolytes effectively suppresses water-induced side reactions and uncontrolled dendrite growth, thereby enhancing the stability and reversibility of Zn plating and stripping.

From a mechanistic perspective, the solvation and desolvation behavior of Zn^{2+} ions plays a critical role in governing interfacial reaction kinetics and deposition morphology. In aqueous electrolytes, Zn^{2+} typically exists in a strongly hydrated coordination environment, most commonly forming octahedral $[Zn(H_2O)_6]^{2+}$ complexes stabilized by hydrogen bonding networks. The desolvation process, which involves partial or complete removal of coordinated water molecules prior to electron transfer, constitutes a key energy barrier that directly influences the nucleation overpotential and charge transfer kinetics at the Zn electrode. This process is highly sensitive to the local coordinated environment and water activity.

The introduction of ion concentration gradients can indirectly modulate Zn^{2+} solvation structures by altering the spatial distribution of ions and solvent molecules near the interface. In regions with elevated Zn^{2+} concentrations, the relative availability of free water molecules decreases, leading to reduced water activity and a higher probability of contact ion pairs or solvent-shared ion configurations[101]. This shift in the coordination environment facilitates partial desolvation and decreases the energy barrier for Zn^{2+} reduction. Conversely, in bulk-like regions with higher water activity, fully hydrated Zn^{2+} species dominate, supporting efficient long-range ion transport. Such spatial variation establishes a progressive desolvation pathway as Zn^{2+} ions migrate toward the electrode, coupling ion transport with solvation dynamics.

Furthermore, water activity not only governs solvation structure but also influences interfacial side reactions, particularly the hydrogen evolution reaction and hydroxide formation. Reduced water activity near the Zn surface suppresses proton reduction and stabilizes the interfacial pH, thereby mitigating parasitic reactions and surface passivation[102]. Therefore, effective gradient engineering should consider not only the Zn^{2+} concentration distribution but also the coupled regulation of coordination chemistry and water activity. This integrated perspective provides a more comprehensive understanding of how gradient structures influence interfacial reaction kinetics and highlights the importance of solvation transport coupling in the design of advanced electrolyte systems for AZBs.

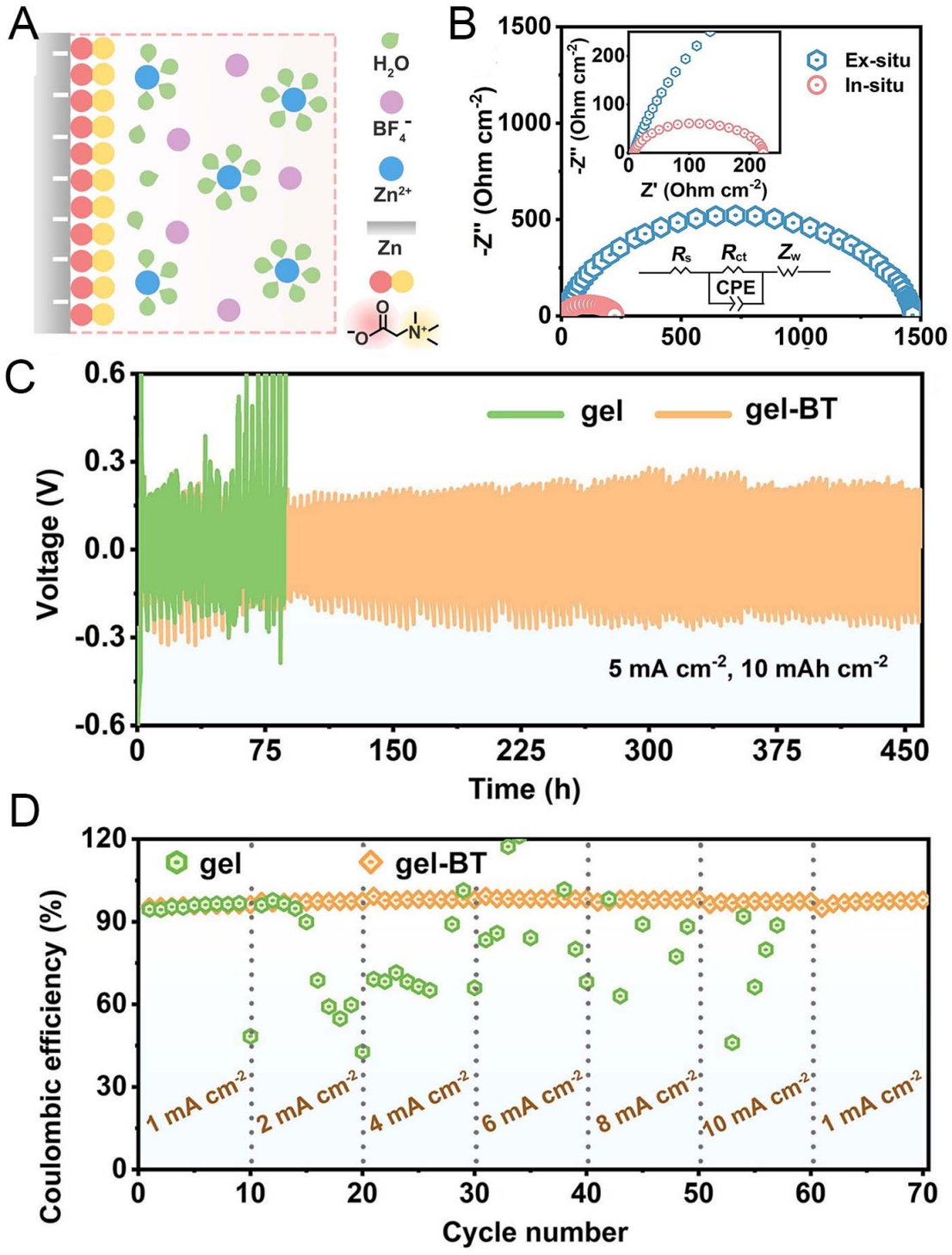

Figure 6. (A) Schematic of the EDL structure following BT addition[100]. (B) EIS profiles of Zn-Zn cells with *ex situ* and *in situ* gel-BT electrolytes[100]. (C) Cycling performance of Zn symmetrical cells with gel and gel-BT electrolytes at 5 mA cm^{-2} and 10 mAh cm^{-2}[100]. (D) Coulombic efficiency of Zn-Cu cells with gel and gel-BT electrolytes at various current densities[100]. (A-D) Reproduced with permission from[100]. Copyright 2024, Elsevier.

Advanced characterization techniques and simulation

In the design of Zn^{2+} concentration gradients, advanced characterization techniques combined with quantitative simulation are indispensable for verifying gradient formation and clarifying how spatial Zn^{2+} distribution regulates interfacial reactions. Electrochemical measurements such as electrochemical

impedance spectroscopy, galvanostatic intermittent titration, chronoamperometry, and transference number tests provide key kinetic parameters, including ionic conductivity, charge transfer resistance, Zn^{2+} diffusion coefficients, and Zn^{2+} transference numbers. These experimentally derived parameters can be incorporated into continuum-scale models based on the Nernst-Planck and Poisson equations or finite element simulations to quantitatively reconstruct Zn^{2+} concentration fields and electric potential distributions across the electrolyte and near the electrode interface[103,104]. It should be clarified that the above two references support the fundamental governing equations and the general modelling framework for metal electrodeposition rather than a specific electrochemical system. Although these studies focus on Li metal systems, the underlying theoretical descriptions, including ion transport, electric field distribution, and interface evolution, are based on general electrochemical principles that are also applicable to Zn deposition. By correlating simulated ion flux profiles with operando or *ex situ* characterization methods such as *in situ* optical microscopy, CLSM, Raman mapping, X-ray photoelectron spectroscopy depth profiling, and electron microscopy of deposited Zn, directly linking gradient-regulated ion transport behavior with nucleation thermodynamics and growth morphology becomes possible. This integrated strategy, in which electrochemical data serve as input parameters for ion transport modelling and are cross-validated by spatially resolved structural and compositional analyses, enables a mechanistic understanding of how engineered Zn^{2+} concentration gradients suppress side reactions, homogenize interfacial current distribution, and stabilize Zn plating and stripping processes.

On the basis of the above strategy, Cui *et al.* designed a viscosity gradient electrolyte configuration by inserting filter paper to spatially divide the electrolyte into a high-viscosity Zn^{2+} ion buffer layer and a low-viscosity bulk transport region, thereby constructing an asymmetric Zn^{2+} concentration regulation pathway[105]. In this architecture, the high viscosity region adjacent to the Zn anode retards Zn^{2+} migration and alleviates local ion depletion, which homogenizes interfacial Zn^{2+} flux and promotes uniform nucleation, whereas the low viscosity region maintains rapid ion transport and low internal resistance. Simulations of Zn^{2+} concentration profiles after charging at 5 mA cm^{-2} for 720 s reveal that the decrease in Zn^{2+} concentration at the cathode surface is nearly identical in both the electrolyte with a Zn^{2+} ion buffer layer and the PVA gel electrolyte, indicating that the thin buffer layer can effectively regulate Zn electrodeposition and induce an ordered Zn^{2+} flux comparable to that of a full gel system [Figure 7A]. Moreover, the Zn^{2+} concentration near the anode in the buffer layer system remains close to that in the liquid electrolyte, confirming its spatially selective regulation behavior, and the opposite side preserves Zn^{2+} conductivity comparable to that of the liquid electrolyte. This asymmetric modulation enables uniform Zn deposition at lower overpotentials and suppresses parasitic reactions. When charged to an areal capacity of 2 mAh cm^{-2} at 5 mA cm^{-2}, Zn deposited in the liquid electrolyte exhibits severe nonuniformity, and pronounced hydrogen bubble accumulation is observed in the gel electrolyte, whereas the viscosity gradient configuration yields dense and uniform Zn without obvious gas evolution, reflecting a stabilized interfacial environment [Figure 7B]. Quantitative analysis of deposition kinetics reveals that the initial deposition area coefficient k_a and the single-step deposition area increase coefficient k_s are lower under viscosity gradient conditions, indicating denser and more reversible Zn growth, whereas the initial Zn^{2+} accumulation coefficient k_m and the hydrogen evolution onset time coefficient p_h are greater, suggesting enhanced Zn^{2+} retention and reduced water activity at the interface [Figure 7C]. The smoother evolution of these parameters further confirms that the constructed Zn^{2+} concentration gradient effectively regulates interfacial reaction dynamics and improves cycling stability.

In addition to reconstructing Zn^{2+} concentration fields through electrochemically derived kinetic parameters and numerical simulations, fluorescence-based visualization techniques offer a direct and spatially resolved approach to probe ion concentration gradients *in situ*. This strategy relies on fluorescent probes whose emission intensity, wavelength shift, or lifetime are sensitive to the local Zn^{2+} concentration or coordination

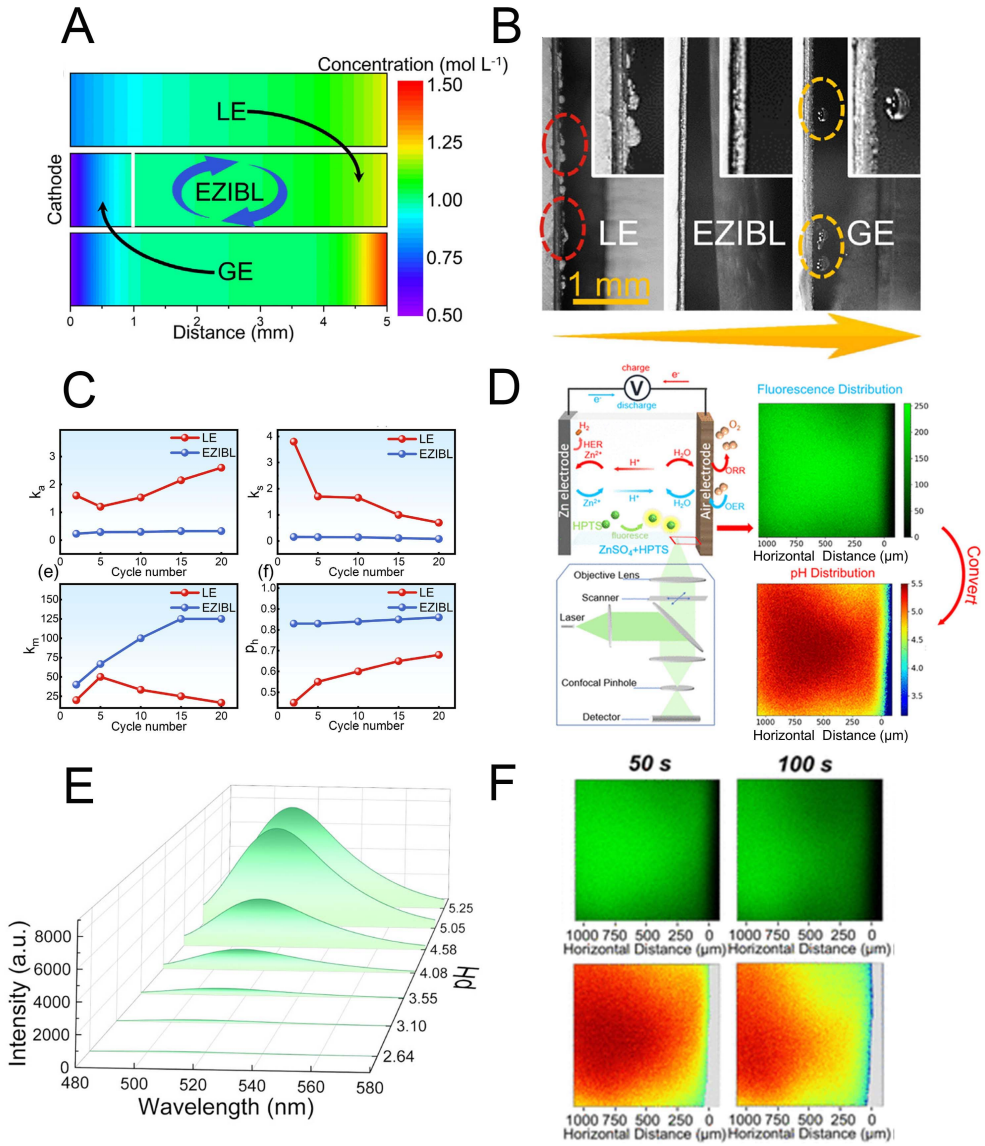

Figure 7. (A) The concentration distribution cloud map of Zn^{2+} in different electrolytes at 5 mA cm^{-2} via numerical simulations[105]. (B) Macroscopic optical observation photographs at 5 mA cm^{-2} and 2 mAh cm^{-2} in different electrolytes[105]. (C) Variation curves of four important parameters (k_a, k_s, k_m, and p_h)[105]. (A-C) Reproduced with permission from[105]. Copyright 2024, KeAi Publishing. (D) Schematic diagram of the observation mechanism using laser scanning confocal microscopy[108]. (E) Fluorescence emission spectra of 1 M $ZnSO_4$ with 500 μM HPTS in the pH range of 2.64 to 5.25[108]. (F) The pH distribution around the air electrode charging at 0.05 mA cm^{-2} obtained by CLSM[108]. (D-F) Reproduced with permission from[108]. Copyright 2024, American Chemical Society.

environment. Upon complexation with Zn^{2+}, the electronic structure of the fluorophore is altered, leading to quantifiable optical responses that can be calibrated to the Zn^{2+} concentration. By integrating such probes into electrolytes or hydrogel matrices and monitoring fluorescence signals via CLSM or operando optical imaging, two-dimensional or three-dimensional maps of Zn^{2+} distribution can be constructed across the electrolyte and near the electrode interface[106,107]. Time-resolved fluorescence imaging further enables the tracking of dynamic concentration evolution during plating and stripping processes, revealing ion depletion, accumulation, and flux heterogeneity under different current densities. When correlated with electrochemical data and modelled ion transport profiles, fluorescence visualization provides complementary validation of gradient formation and clarifies how localized Zn^{2+} enrichment or depletion governs nucleation behavior, interfacial stability, and dendrite growth. This combined optical and electrochemical methodology, therefore, establishes a powerful platform for elucidating the mechanistic role of engineered Zn^{2+}

concentration gradients in AZBs.

On the basis of the above mechanism, Chen *et al.* introduced CLSM to realize operando visualization of ion transport by coupling fluorescence imaging with electrochemical processes in a neutral Zn air battery model system[108]. A pH-sensitive fluorescent probe was employed to convert local ion transport-induced fluctuations in pH into measurable optical signals, thereby enabling indirect mapping of interfacial ion dynamics [Figure 7D]. After immersion in the $ZnSO_4$ electrolyte, pronounced fluctuations in the pH with pulsation behavior were observed near the Zn electrode, reflecting severe hydrogen evolution and periodic variations in reaction intensity, whereas a galvanized Zn electrode exhibited much smaller fluctuations in the pH, indicating improved corrosion resistance and suppressed parasitic reactions. At the air electrode, distinct spatial heterogeneity in ion transport was detected during both discharge and charge, and with increasing current density, the dominant transport mode gradually shifted from diffusion-controlled to convection diffusion-coupled behavior, highlighting the increasing contribution of convection to internal ion migration. To establish a quantitative relationship between the fluorescence response and pH, the emission spectra of an electrolyte containing 1 M $ZnSO_4$ and 500 μM 8-hydroxypyrene 1,3,6-trisulfonic acid trisodium salt were recorded under 458 nm excitation with emission collected from 480 to 580 nm [Figure 7E]. The fluorescence intensity increased monotonically with increasing pH and reached a maximum at approximately 510 nm, providing a calibration basis for confocal imaging. On the basis of this correlation, *in situ* imaging during charging revealed that the fluorescence intensity near the electrode decreased within the first 50 to 100 s, indicating a transient local pH decrease caused by the diffusion of alkaline species into the bulk electrolyte [Figure 7F]. These results demonstrate that fluorescence-based operando microscopy can be used to quantitatively visualize dynamic ion concentration gradients and elucidate interfacial transport mechanisms in Zn-based electrochemical systems.

Building upon the insights provided by advanced characterization techniques and simulation methods, it becomes possible to move beyond individual case analyses toward a more unified understanding of ion-concentration gradient engineering. By quantitatively resolving Zn^{2+} transport behavior, interfacial reaction kinetics, and spatial concentration distributions, these approaches enable direct comparisons across different gradient design strategies[109]. Despite variations in material systems and structural configurations, the underlying regulatory mechanisms can be broadly categorized into ion transport modulation, solvation structure tuning, and interfacial electric field homogenization. For example, additive-based systems primarily influence Zn^{2+} coordination environments and electric double layer structures, whereas separator and hydrogel-based systems impose spatial confinement and directional ion pathways, leading to distinct gradient formation modes ranging from interfacial Zn^{2+} enrichment to continuous concentration profiles across the electrolyte[110].

Importantly, the effectiveness of these strategies can be quantitatively evaluated through key electrochemical and transport parameters extracted from combined experimental and modelling analyses. Metrics such as the Zn^{2+} transference number, nucleation overpotential, interfacial resistance, and chronoamperometric response provide direct insight into the ion flux uniformity and interfacial stability[111]. Moreover, performance indicators, including critical current density, Coulombic efficiency, and long-term cycling stability, reflect the practical impact of gradient regulation on suppressing dendrite growth and parasitic reactions. These quantitative descriptors establish a direct link between the gradient structure, ion transport behavior, and electrochemical performance. On the basis of these correlations, effective gradient engineering should simultaneously regulate interfacial Zn^{2+} flux while preserving sufficient bulk ionic conductivity, thereby balancing interfacial stability with overall transport efficiency. This integrated understanding, enabled by advanced characterization and simulation, provides general design principles for the rational development of high-performance aqueous Zn-based batteries.

Despite the significant progress achieved with advanced characterization techniques such as fluorescence imaging and CLSM, several limitations remain that should be carefully considered when experimental results are interpreted. First, the spatial resolution of these techniques is fundamentally constrained by optical diffraction limits, which may hinder accurate probing of the nanoscale ion distribution and interfacial structures. Second, the quantitative reliability of fluorescence-based methods depends strongly on probe calibration, local environmental sensitivity, and potential interference from factors such as pH variation, ionic strength, and probe aggregation, which can introduce uncertainties in correlating signal intensity with actual Zn^{2+} concentration. In addition, these techniques typically rely on exogenous probes that may perturb the native electrolyte environment or alter ion transport behavior.

Furthermore, capturing rapid and transient ion transport processes under practical operating conditions remains challenging because of limitations in temporal resolution and signal acquisition speed. As a result, experimentally observed concentration profiles may represent time-averaged or partially evolved states rather than true instantaneous distributions[90]. To address these challenges, future efforts should focus on integrating high-resolution operando techniques with quantitative calibration strategies and complementary methods such as electrochemical modelling and spectroscopy. Such multimodal approaches are essential for achieving reliable, spatially resolved, and quantitatively accurate characterization of Zn^{2+} concentration gradients and interfacial processes in AZBs.

CONCLUSION AND OUTLOOK

To provide a clearer comparison of representative strategies and facilitate the extraction of general design principles, key studies are summarized in Table 1. Despite differences in electrolyte composition and structural design, these approaches consistently rely on spatial regulation of Zn^{2+} distribution to control interfacial behavior. This review demonstrates that ion concentration gradient engineering represents a unifying and mechanism-driven strategy for regulating zinc electrode interfacial reactions in aqueous Zn-based batteries (AZBs). Across both liquid and hydrogel electrolyte systems, diverse material designs converge toward a common objective: spatial control of Zn^{2+} transport and interfacial ion distribution. In liquid electrolytes, gradients are primarily established through selective ion-additive interactions and ion-selective separators, which reshape Zn^{2+} solvation structures and electric double layers. In hydrogel electrolytes, gradient regulation is achieved via heterogeneous polymer networks, asymmetric compositions, covalent anchoring, and additive-assisted confinement, enabling localized control over ion mobility, water activity, and desolvation kinetics. Despite differences in material form, these strategies share several core mechanistic features: (i) buffering Zn^{2+} migration to avoid local depletion or accumulation, (ii) homogenizing interfacial Zn^{2+} flux to promote uniform nucleation and growth, and (iii) reducing interfacial water activity to suppress parasitic reactions. Importantly, recent advances in advanced characterization techniques, including concentration-field simulations, parameterized electrochemical analysis, and operando fluorescence visualization, have enabled direct observation of Zn^{2+} distribution and its temporal evolution, providing compelling evidence that interfacial stability is intrinsically linked to controlled concentration gradients rather than static material properties alone.

Although significant progress has been made in ion concentration gradient engineering, several key challenges must still be addressed to fully realize its practical potential in AZBs. First, most reported gradient structures are intrinsically static, whereas Zn deposition and stripping involve highly dynamic processes accompanied by the continuous evolution of local electric fields, ion flux, and interfacial chemistry during prolonged cycling and at high current densities. The development of self-adaptive or dynamically regulated gradient systems that can maintain stable ion distributions under realistic operating conditions is therefore important. Second, the lack of quantitative and real-time characterization of local Zn^{2+} concentration, water activity, and interfacial chemical states limits the establishment of definitive structure-function relationships.

Table 1. Zn^{2+} concentration gradient regulation methods described in this review

Strategy type	Electrolyte system	Gradient construction strategy	Dominant mechanism	Current density	Cycling performance
Additive-based (N,S-doped quantum dots, NSQDs)[71]	ZnSO4 + NSQDs	Interfacial adsorption-induced Zn^{2+} enrichment	Coordination + electric double layer (EDL) regulation	10 A g^{-1}	208.4 mAh g^{-1} (*vs.* 44.4 mAh g^{-1} baseline); high reversibility
Additive-based (diethyl phosphoramidate, DP)[77]	$ZnSO_4$ + DP	Hydrogen bond modulation + gradient solid electrolyte interphase (SEI) formation	Solvation reconstruction + reduced water activity	5 mA cm^{-2}	Uniform deposition; improved rate capability
Functional separator (bacterial cellulose-filter paper, BC-FP)[82]	$ZnSO_4$ + BC/FP	Ion-selective transport + gradient pore structure	Zn^{2+} flux homogenization + nanoconfinement	1 mA cm^{-2}	Smooth Zn morphology; enhanced rate performance
Solvent-regulating separator (gradient hydrophilic cellulose)[85]	$ZnSO_4$ + modified cellulose separator	Water distribution gradient	Solvation tuning + suppressed hydrogen evolution reaction (HER)	-	Improved capacity and cycling stability
Gradient hydrogel (polyvinyl alcohol/cellulose nanofiber/graphene oxide, PVA/CNF/GO)[91]	PVA/CNF/GO hydrogel	Crosslinking density gradient	Ion transport regulation + progressive desolvation	0.15-3 A g^{-1}	250.6 → 89.7 mAh g^{-1}; superior to homogeneous gels
Gradient hydrogel networks (GHNs) *vs.* homogeneous hydrogel networks (HHNs)[90]	Covalently anchored polymer/Zn	Epitaxial polymerization + charge density gradient	Selective ion transport + 3D diffusion	0.1-2 A g^{-1}	67 → 44 mAh g^{-1}; higher than HHNs
Layered concentration-gradient electrolyte (high-concentration electrolyte@carboxymethyl cellulose, HCE@CMC)[95]	HCE@CMC + dilute electrolyte	Anode-to-separator concentration gradient	Water activity regulation + Zn^{2+} flux control	-	92 mAh g^{-1} after 800 cycles (*vs.* 37 mAh g^{-1} after 200 cycles)
Asymmetric hydrogel electrolyte (AHE) for Zn-I_2 batteries[96]	Carra-Zn-Alg + PVA-PEDOT	Dual-region functional hydrogel	Zn^{2+} transport regulation + polyiodide confinement	0.1-10 A g^{-1}	210 → 150 mAh g^{-1}; capacity recovery at low current
Additive-functionalized hydrogel (betaine, BT)[100]	Hydrogel + BT	Interfacial adsorption + electric double layer reconstruction	Hybrid SEI formation + water exclusion	5 mA cm^{-2}	450 h stable cycling; high CE (1-10 mA cm^{-2})
Electrolyte with Zn^{2+} ion buffer layer (EZIBL)[105]	High/low viscosity electrolyte	Viscosity gradient via ion buffer layer	Flux buffering + diffusion regulation	5 mA cm^{-2}	Uniform deposition; suppressed HER; stable cycling

Future studies should integrate advanced operando characterization techniques with electrochemical parameter extraction and numerical modelling to quantitatively correlate ion transport behavior with interfacial reaction mechanisms. Third, a fundamental trade-off remains between interfacial ion regulation and bulk ion transport efficiency. While highly restrictive gradients may suppress dendrite growth, they can also introduce concentration polarization, whereas highly conductive systems may weaken gradient regulation effects. Rational design strategies that spatially decouple bulk ion transport from interfacial ion modulation will therefore be crucial for optimizing both reaction kinetics and mass transport. Finally, many currently reported gradient electrolyte systems rely on complex architectures or sophisticated fabrication processes, which may hinder scalability and practical deployment. Future efforts should thus emphasize simplified and scalable fabrication strategies and evaluate battery performance under practical conditions, including high areal capacities and lean electrolyte configurations.

Ultimately, ion concentration gradient engineering should be viewed not as a material optimization problem alone but as a spatiotemporal regulation strategy for electrochemical interfaces. By combining rational gradient design with advanced characterization and dynamic regulation concepts, future research can bridge the gap between mechanistic understanding and practical deployment, accelerating the development of

durable, high-rate, and commercially viable AZBs.

DECLARATIONS

Author contributions

Conceptualization, funding acquisition, supervision, writing-review & editing: Cui, Y.
Investigation: Jin, Z.; Yu, X.
Supervision, writing-review & editing: He, Y.
Supervision, project administration, review & editing: Yang, X.

Availability of data and materials

Not applicable.

AI and AI-assisted tools statement

Not applicable.

Conflicts of interest

All authors declared that there are no conflicts of interest.

Financial support and sponsorship

The authors are thankful for the funding support from the Talent Project of Hefei University (25RC36).

Ethical approval and consent to participate

Not applicable.

Consent for publication

Not applicable.

REFERENCES

1. Shang, W.; Yu, W.; Liu, Y.; et al. Rechargeable alkaline zinc batteries: progress and challenges. *Energy. Storage. Mater.* **2020**, *31*, 44-57. DOI
2. Yu, F.; Pang, L.; Wang, X.; et al. Aqueous alkaline-acid hybrid electrolyte for zinc-bromine battery with 3V voltage window. *Energy. Storage. Mater.* **2019**, *19*, 56-61. DOI
3. Tan, P.; Chen, B.; Xu, H.; et al. Flexible Zn- and Li-air batteries: recent advances, challenges, and future perspectives. *Energy. Environ. Sci.* **2017**, *10*, 2056-80. DOI
4. Shang, W.; Yu, W.; Tan, P.; et al. Achieving high energy density and efficiency through integration: progress in hybrid zinc batteries. *J. Mater. Chem. A.* **2019**, *7*, 15564-74. DOI
5. Khan, Z.; Kumar, D.; Crispin, X. Does water-in-salt electrolyte subdue issues of Zn batteries? *Adv. Mater.* **2023**, *35*, 2300369. DOI PubMed
6. Sui, Y.; Ji, X. Anticatalytic strategies to suppress water electrolysis in aqueous batteries. *Chem. Rev.* **2021**, *121*, 6654-95. DOI PubMed
7. Fang, G.; Zhou, J.; Pan, A.; Liang, S. Recent advances in aqueous zinc-ion batteries. *ACS. Energy. Lett.* **2018**, *3*, 2480-501. DOI
8. Wang, T.; Li, C.; Xie, X.; et al. Anode materials for aqueous zinc ion batteries: mechanisms, properties, and perspectives. *ACS. Nano.* **2020**, *14*, 16321-47. DOI
9. Ruan, P.; Liang, S.; Lu, B.; Fan, H. J.; Zhou, J. Design strategies for high-energy-density aqueous zinc batteries. *Angew. Chem. Int. Ed.* **2022**, *61*, e202200598. DOI
10. Lin, D.; Li, Y. Recent advances of aqueous rechargeable zinc-iodine batteries: challenges, solutions, and prospects. *Adv. Mater.* **2022**, *34*, 2108856. DOI
11. Yu, W.; Shang, W.; Tan, P.; et al. Toward a new generation of low cost, efficient, and durable metal-air flow batteries. *J. Mater. Chem. A.* **2019**, *7*, 26744-68. DOI
12. Song, M.; Tan, H.; Chao, D.; Fan, H. J. Recent advances in Zn-ion batteries. *Adv. Funct. Mater.* **2018**, *28*, 1802564. DOI

13. Lee, J. S.; Tai, Kim. S.; Cao, R.; et al. Metal-air batteries with high energy density: Li-air versus Zn-Air. *Adv. Energy. Mater.* **2010**, *1*, 34-50. DOI
14. Zeng, X.; Hao, J.; Wang, Z.; Mao, J.; Guo, Z. Recent progress and perspectives on aqueous Zn-based rechargeable batteries with mild aqueous electrolytes. *Energy. Storage. Mater.* **2019**, *20*, 410-37. DOI
15. Zeng, Y.; Zhang, X.; Qin, R.; et al. Dendrite-free zinc deposition induced by multifunctional CNT frameworks for stable flexible Zn-ion batteries. *Adv. Mater.* **2019**, *31*, 1903675. DOI
16. Yang, Q.; Li, Q.; Liu, Z.; et al. Dendrites in Zn-based batteries. *Adv. Mater.* **2020**, *32*, 2001854. DOI
17. Tian, Y.; An, Y.; Wei, C.; et al. Flexible and free-standing $Ti_3C_2T_x$ MXene@Zn paper for dendrite-free aqueous zinc metal batteries and nonaqueous lithium metal batteries. *ACS. Nano.* **2019**, *13*, 11676-85. DOI
18. Yu, J.; Yu, W.; Zhang, Z.; Tan, P. Reunderstanding the uneven deposition in aqueous zinc-based batteries. *Chem. Eng. J.* **2024**, *481*, 148556. DOI
19. Liu, B.; Yuan, X.; Li, Y. Colossal capacity loss during calendar aging of Zn battery chemistries. *ACS. Energy. Lett.* **2023**, *8*, 3820-8. DOI
20. Song, Y.; Xia, L.; Salla, M.; et al. A hybrid redox-mediated zinc-air fuel cell for scalable and sustained power generation. *Angew. Chem. Int. Ed.* **2024**, *63*, e202314796. DOI
21. Wang, Z.; Huang, J.; Guo, Z.; et al. A metal-organic framework host for highly reversible dendrite-free zinc metal anodes. *Joule* **2019**, *3*, 1289-300. DOI
22. Ma, L.; Chen, S.; Li, N.; et al. Hydrogen-free and dendrite-free all-solid-state Zn-ion batteries. *Adv. Mater.* **2020**, *32*, 1908121. DOI
23. Bockelmann, M.; Becker, M.; Reining, L.; Kunz, U.; Turek, T. Passivation of zinc anodes in alkaline electrolyte: part I. Determination of the starting point of passive film formation. *J. Electrochem. Soc.* **2018**, *165*, A3048-55. DOI
24. Thomas, S.; Cole, I.; Sridhar, M.; Birbilis, N. Revisiting zinc passivation in alkaline solutions. *Electrochim. Acta.* **2013**, *97*, 192-201. DOI
25. Zhou, M.; Guo, S.; Fang, G.; et al. Suppressing by-product via stratified adsorption effect to assist highly reversible zinc anode in aqueous electrolyte. *J. Energy. Chem.* **2021**, *55*, 549-56. DOI
26. Wittman, R. M.; Sacci, R. L.; Zawodzinski, T. A. Elucidating mechanisms of oxide growth and surface passivation on zinc thin film electrodes in alkaline solutions using the electrochemical quartz crystal microbalance. *J. Power. Sources.* **2019**, *438*, 227034. DOI
27. Ma, L.; Li, Q.; Ying, Y.; et al. Toward practical high-areal-capacity aqueous zinc-metal batteries: quantifying hydrogen evolution and a solid-ion conductor for stable zinc anodes. *Adv. Mater.* **2021**, *33*, 2007406. DOI
28. He, Y.; Shang, W.; Ni, M.; Huang, Y.; Zhao, H.; Tan, P. In-situ observation of the gas evolution process on the air electrode of Zn-air batteries during charging. *Chem. Eng. J.* **2022**, *427*, 130862. DOI
29. He, Y.; Cui, Y.; Shang, W.; Zhao, Z.; Tan, P. Insight into potential oscillation behaviors during Zn electrodeposition: Mechanism and inspiration for rechargeable Zn batteries. *Chem. Eng. J.* **2022**, *438*, 135541. DOI
30. Liu, B.; Xu, Z.; Wei, C.; et al. Re-understanding and mitigating hydrogen release chemistry toward reversible aqueous zinc metal batteries. *eScience* **2025**, *5*, 100330. DOI
31. Zhao, Q.; Yu, X.; Xue, J.; et al. Competitive tradeoff between Zn deposition and hydrogen evolution reaction on Zn-metal anode. *ACS. Energy. Lett.* **2024**, *9*, 4102-10. DOI
32. Meng, Q.; Bai, Q.; Zhao, R.; et al. Attenuating water activity through impeded proton transfer resulting from hydrogen bond enhancement effect for fast and ultra-stable Zn metal anode. *Adv. Energy. Mater.* **2023**, *13*, 2302828. DOI
33. Jin, S.; Chen, P.; Qiu, Y.; et al. Zwitterionic polymer gradient interphases for reversible zinc electrochemistry in aqueous alkaline electrolytes. *J. Am. Chem. Soc.* **2022**, *144*, 19344-52. DOI
34. Han, Y.; Wang, F.; Zhang, B.; et al. Building block effect induces horizontally oriented bottom Zn(002) deposition for a highly stable zinc anode. *Energy. Storage. Mater.* **2023**, *62*, 102928. DOI
35. Meng, Y.; Wang, M.; Xu, J.; et al. Balancing interfacial reactions through regulating *p*-band centers by an indium tin oxide protective layer for stable Zn metal anodes. *Angew. Chem. Int. Ed.* **2023**, *62*, e202308454. DOI
36. Duan, J.; Dong, J.; Cao, R.; et al. Regulated Zn plating and stripping by a multifunctional polymer-alloy interphase layer for stable Zn metal anode. *Adv. Sci.* **2023**, *10*, 2303343. DOI PubMed PMC
37. Zhou, Y.; Xia, J.; Di, J.; et al. Ultrahigh-rate Zn stripping and plating by capacitive charge carriers enrichment boosting Zn-based energy storage. *Adv. Energy. Mater.* **2023**, *13*, 2203165. DOI
38. Wang, T.; Wang, P.; Pan, L.; et al. Stabling zinc metal anode with polydopamine regulation through dual effects of fast desolvation and ion confinement. *Adv. Energy. Mater.* **2022**, *13*, 2203523. DOI
39. Dong, H.; Hu, X.; Liu, R.; et al. Bio-inspired polyanionic electrolytes for highly stable zinc-ion batteries. *Angew. Chem. Int. Ed.* **2023**, *62*, e202311268. DOI PubMed PMC
40. Naveed, A.; Yang, H.; Yang, J.; Nuli, Y.; Wang, J. Highly reversible and rechargeable safe Zn batteries based on a triethyl phosphate electrolyte. *Angew. Chem. Int. Ed.* **2019**, *58*, 2760-4. DOI PubMed

41. Yan, M.; Dong, N.; Zhao, X.; Sun, Y.; Pan, H. Tailoring the stability and kinetics of Zn anodes through trace organic polymer additives in dilute aqueous electrolyte. *ACS. Energy. Lett.* **2021**, *6*, 3236-43. DOI
42. Han, D.; Cui, C.; Zhang, K.; et al. A non-flammable hydrous organic electrolyte for sustainable zinc batteries. *Nat. Sustain.* **2021**, *5*, 205-13. DOI
43. Zhu, Q.; Sun, G.; Qiao, S.; et al. Selective shielding of the (002) plane enabling vertically oriented zinc plating for dendrite-free zinc anode. *Adv. Mater.* **2023**, *36*, 2308577. DOI
44. Zhou, L.; Yang, R.; Xu, S.; et al. Maximizing electrostatic polarity of non-sacrificial electrolyte additives enables stable zinc-metal anodes for aqueous batteries. *Angew. Chem. Int. Ed.* **2023**, *62*, e202307880. DOI
45. Cao, Z.; Zhuang, P.; Zhang, X.; Ye, M.; Shen, J.; Ajayan, P. M. Strategies for dendrite-free anode in aqueous rechargeable zinc ion batteries. *Adv. Energy. Mater.* **2020**, *10*, 2001599. DOI
46. Li, Y.; Jia, H.; Ali, U.; et al. Successive gradient internal electric field strategy toward dendrite-free zinc metal anode. *Adv. Energy. Mater.* **2023**, *13*, 2301643. DOI
47. Wang, D.; Liu, H.; Lv, D.; Wang, C.; Yang, J.; Qian, Y. Rational screening of artificial solid electrolyte interphases on Zn for ultrahigh-rate and long-life aqueous batteries. *Adv. Mater.* **2022**, *35*, 2207908. DOI
48. Gao, Y.; Cao, Q.; Pu, J.; et al. Stable Zn anodes with triple gradients. *Adv. Mater.* **2022**, *35*, 2207573. DOI
49. Liu, Q.; Yu, Z.; Zhou, R.; Zhang, B. A semi-liquid electrode toward stable Zn powder anode. *Adv. Funct. Mater.* **2022**, *33*, 2210290. DOI
50. Yuan, W.; Nie, X.; Ma, G.; et al. Realizing textured zinc metal anodes through regulating electrodeposition current for aqueous zinc batteries. *Angew. Chem. Int. Ed.* **2023**, *62*, e202218386. DOI
51. Garcia, G.; Ventosa, E.; Schuhmann, W. Complete prevention of dendrite formation in Zn metal anodes by means of pulsed charging protocols. *ACS. Appl. Mater. Interfaces.* **2017**, *9*, 18691-8. DOI PubMed
52. He, Y.; Cui, Y.; Zhao, Z.; Chen, Y.; Shang, W.; Tan, P. Strategies for bubble removal in electrochemical systems. *Energy. Rev.* **2023**, *2*, 100015. DOI
53. Yang, Q.; Liang, G.; Guo, Y.; et al. Do zinc dendrites exist in neutral zinc batteries: a developed electrohealing strategy to in situ rescue in-service batteries. *Adv. Mater.* **2019**, *31*, 1903778. DOI
54. Yu, W.; Shang, W.; Xiao, X.; et al. Achieving a stable zinc electrode with ultralong cycle life by implementing a flowing electrolyte. *J. Power. Sources.* **2020**, *453*, 227856. DOI
55. García-gaitán, E.; Morant-miñana, M. C.; Frattini, D.; et al. Agarose-based gel electrolytes for sustainable primary and secondary zinc-air batteries. *Chem. Eng. J.* **2023**, *472*, 144870. DOI
56. Wang, W.; Tang, M.; Zheng, Z.; Chen, S. Alkaline polymer membrane-based ultrathin, flexible, and high-performance solid-state Zn-air battery. *Adv. Energy. Mater.* **2019**, *9*, 1901718. DOI
57. Tian, C.; Wang, J.; Sun, R.; et al. Improved interfacial ion migration and deposition through the chain-liquid synergistic effect by a carboxylated hydrogel electrolyte for stable zinc metal anodes. *Angew. Chem. Int. Ed.* **2023**, *62*, e202310970. DOI
58. Qiu, B.; Liang, K.; Huang, W.; et al. Crystal-facet manipulation and interface regulation via TMP-modulated solid polymer electrolytes toward high-performance Zn metal batteries. *Adv. Energy. Mater.* **2023**, *13*, 2301193. DOI
59. Zheng, G.; Yan, T.; Hong, Y.; et al. A non-Newtonian fluid quasi-solid electrolyte designed for long life and high safety Li-O_2 batteries. *Nat. Commun.* **2023**, *14*, 2268. DOI PubMed PMC
60. Kang, L.; Cui, M.; Jiang, F.; et al. Nanoporous $CaCO_3$ coatings enabled uniform Zn stripping/plating for long-life zinc rechargeable aqueous batteries. *Adv. Energy. Mater.* **2018**, *8*, 1801090. DOI
61. Yu, L.; Huang, J.; Wang, S.; Qi, L.; Wang, S.; Chen, C. Ionic liquid “water pocket” for stable and environment-adaptable aqueous zinc metal batteries. *Adv. Mater.* **2023**, *35*, 2210789. DOI
62. Thorat, G. M.; Lee, H.; Kim, J. H.; Kwon, O.; Mun, J. Highly reversible Zn metal anode with V-shaped valley-like nanoarray structure for rechargeable Zn-ion aqueous batteries. *J. Electrochem. Sci. Technol.* **2025**, *16*, 236-48. DOI
63. Wang, S.; Wang, Z.; Yin, Y.; et al. A highly reversible zinc deposition for flow batteries regulated by critical concentration induced nucleation. *Energy. Environ. Sci.* **2021**, *14*, 4077-84. DOI
64. Song, Z. S.; Ding, J.; Liu, B.; et al. A rechargeable Zn-air battery with high energy efficiency and long life enabled by a highly water-retentive gel electrolyte with reaction modifier. *Adv. Mater.* **2020**, *32*, 1908127. DOI
65. Chen, Z.; Wang, T.; Hou, Y.; et al. Polymeric single-ion conductors with enhanced side-chain motion for high-performance solid zinc-ion batteries. *Adv. Mater.* **2022**, *34*, 2207682. DOI
66. Cheng, Y.; Jiao, Y.; Wu, P. Manipulating Zn 002 deposition plane with zirconium ion crosslinked hydrogel electrolyte toward dendrite free Zn metal anodes. *Energy. Environ. Sci.* **2023**, *16*, 4561-71. DOI
67. Ye, Z.; Cao, Z.; Lam, Chee. M. O.; et al. Advances in Zn-ion batteries via regulating liquid electrolyte. *Energy. Storage. Mater.* **2020**, *32*, 290-305. DOI

68. Fu, C.; Wang, Y.; Lu, C.; et al. Modulation of hydrogel electrolyte enabling stable zinc metal anode. *Energy. Storage. Mater.* **2022**, *51*, 588-98. DOI
69. Duan, G.; Wang, Y.; Luo, B.; et al. Taurine-mediated dynamic bridging strategy for highly stable Zn metal anode. *Energy. Storage. Mater.* **2023**, *61*, 102882. DOI
70. Zhang, Q.; Luan, J.; Fu, L.; et al. The three-dimensional dendrite-free zinc anode on a copper mesh with a zinc-oriented polyacrylamide electrolyte additive. *Angew. Chem. Int. Ed.* **2019**, *58*, 15841-7. DOI
71. Wang, F.; Lu, H.; Zhu, H.; et al. Mitigating the interfacial concentration gradient by negatively charged quantum dots toward dendrite-free Zn anodes. *Energy. Storage. Mater.* **2023**, *58*, 215-21. DOI
72. Zhou, J.; Xie, M.; Wu, F.; et al. Ultrathin surface coating of nitrogen-doped graphene enables stable zinc anodes for aqueous zinc-ion batteries. *Adv. Mater.* **2021**, *33*, 2101649. DOI
73. Zeng, Y.; Sun, P. X.; Pei, Z.; et al. Nitrogen-doped carbon fibers embedded with zincophilic Cu nanoboxes for stable Zn-metal anodes. *Adv. Mater.* **2022**, *34*, 2200342. DOI
74. Wang, C.; Liu, Y.; Qu, X.; et al. Ultra-stretchable and fast self-healing ionic hydrogel in cryogenic environments for artificial nerve fiber. *Adv. Mater.* **2022**, *34*, 2105416. DOI
75. Jiang, R.; Naren, T.; Chen, Y.; et al. Enhanced hydrogen bonding through strong water-locking additives for long-term cycling of zinc ion batteries. *Adv. Funct. Mater.* **2024**, *34*, 2411477. DOI
76. Shi, Z.; Li, M.; Fu, X.; Zhang, Y.; Jiao, S.; Zhao, Y. Bimodal block molecule with ether-type and hydroxyl-type oxygen stabilizes Zn anode in super-dilute electrolyte. *Adv. Funct. Mater.* **2024**, *34*, 2316427. DOI
77. Zong, Q.; Liu, X.; Zhang, Q.; et al. Interfacial gradient engineering synergized with self-adaptive cathodic defense for durable Zn-ion batteries. *Energy. Environ. Sci.* **2025**, *18*, 8256-67. DOI
78. Wu, A.; Zhang, S.; Li, Q.; et al. Multifunctional crown ether additive regulates desolvation process to achieve highly reversible zinc-metal batteries. *Adv. Energy. Mater.* **2025**, *15*, 2404450. DOI
79. Wang, P.; Li, T. C.; Liu, Y.; et al. Targeted docking of localized hydrogen bond for efficient and reversible zinc-ion batteries. *Angew. Chem. Int. Ed.* **2025**, *137*, e202422547. DOI
80. Bannon, S. M.; Geise, G. M. Influence of Donnan and dielectric exclusion on ion sorption in sulfonated polysulfones. *J. Membr. Sci.* **2024**, *694*, 122396. DOI
81. Kim, H.; Lim, J.; Lee, H.; Eom, S.; Hong, Y. T.; Lee, S. Artificially engineered, bicontinuous anion-conducting/-repelling polymeric phases as a selective ion transport channel for rechargeable zinc-air battery separator membranes. *J. Mater. Chem. A.* **2016**, *4*, 3711-20. DOI
82. Liu, Z.; Liu, Q.; Mo, H.; et al. Gradient cellulose-based separator with dual nano-confinement and ion-guiding functions for dendrite-free zinc-ion batteries. *Chem. Eng. J.* **2025**, *523*, 168579. DOI
83. Wang, Y.; Long, J.; Hu, J.; Sun, Z.; Meng, L. Polyvinyl alcohol/Lyocell dual-layer paper-based separator for primary zinc-air batteries. *J. Power. Sources.* **2020**, *453*, 227853. DOI
84. Hu, Q.; Hu, J.; Ma, F.; et al. Redistributing zinc-ion flux by work function chemistry toward stabilized and durable Zn metal batteries. *Energy. Environ. Sci.* **2024**, *17*, 2554-65. DOI
85. Dong, Y.; Fan, W.; Wang, X.; et al. Hydrophobicity gradient in ultrathin cellulose separators for durable seawater-based zinc batteries. *Adv. Funct. Mater.* **2025**, *36*, e13685. DOI
86. Liu, Z.; Li, G.; Xi, M.; et al. Interfacial engineering of Zn metal via a localized conjugated layer for highly reversible aqueous zinc ion battery. *Angew. Chem. Int. Ed.* **2024**, *63*, e202319091. DOI
87. Zhou, J.; Cheng, J.; Wang, B.; Peng, H.; Lu, J. Flexible metal-gas batteries: a potential option for next-generation power accessories for wearable electronics. *Energy. Environ. Sci.* **2020**, *13*, 1933-70. DOI
88. Wang, Z.; Li, H.; Tang, Z.; et al. Hydrogel electrolytes for flexible aqueous energy storage devices. *Adv. Funct. Mater.* **2018**, *28*, 1804560. DOI
89. Zhu, K.; Niu, X.; Xie, W.; et al. An integrated Janus hydrogel with different hydrophilicities and gradient pore structures for high-performance zinc-ion batteries. *Energy. Environ. Sci.* **2024**, *17*, 4126-36. DOI
90. Cui, Y.; Chen, W.; Xin, W.; et al. Gradient quasi-solid electrolyte enables selective and fast ion transport for robust aqueous zinc-ion batteries. *Adv. Mater.* **2023**, *36*, 2308639. DOI
91. Wang, Q.; Huang, J.; Qi, L.; et al. A bioinspired gradient hydrogel electrolyte network with optimized interfacial chemistry toward robust aqueous zinc-ion batteries. *ACS. Nano.* **2025**, *19*, 26770-81. DOI
92. Qin, Y.; Li, H.; Han, C.; Mo, F.; Wang, X. Chemical welding of the electrode-electrolyte interface by Zn-metal-initiated in situ gelation for ultralong-life Zn-ion batteries. *Adv. Mater.* **2022**, *34*, 2207118. DOI
93. Ma, L.; Chen, S.; Wang, D.; et al. Super-stretchable zinc-air batteries based on an alkaline-tolerant dual-network hydrogel electrolyte. *Adv. Energy. Mater.* **2019**, *9*, 1803046. DOI

94. Sun, N.; Lu, F.; Yu, Y.; Su, L.; Gao, X.; Zheng, L. Alkaline double-network hydrogels with high conductivities, superior mechanical performances, and antifreezing properties for solid-state zinc-air batteries. *ACS. Appl. Mater. Interfaces.* **2020**, *12*, 11778-88. DOI
95. Lu, H.; Zhang, D.; Jin, Q.; et al. Gradient electrolyte strategy achieving long-life zinc anodes. *Adv. Mater.* **2023**, *35*, 2300620. DOI
96. Liu, Q.; Yu, Z.; Fan, K.; Huang, H.; Zhang, B. Asymmetric hydrogel electrolyte featuring a customized anode and cathode interfacial chemistry for advanced Zn-I_2 batteries. *ACS. Nano.* **2024**, *18*, 22484-94. DOI
97. Nguyen, T. N.; Iranpour, B.; Cheng, E.; Madden, J. D. W. Washable and stretchable Zn-MnO_2 rechargeable cell. *Adv. Energy. Mater.* **2021**, *12*, 2103148. DOI
98. Wang, M.; Xu, N.; Fu, J.; Liu, Y.; Qiao, J. High-performance binary cross-linked alkaline anion polymer electrolyte membranes for all-solid-state supercapacitors and flexible rechargeable zinc-air batteries. *J. Mater. Chem. A.* **2019**, *7*, 11257-64. DOI
99. Fan, X.; Wang, H.; Liu, X.; et al. Functionalized nanocomposite gel polymer electrolyte with strong alkaline-tolerance and high zinc anode stability for ultralong-life flexible zinc-air batteries. *Adv. Mater.* **2022**, *35*, 2209290. DOI
100. Liu, Z.; Zhang, W.; Yin, H.; et al. Gradient solid electrolyte interphase exerted by robust hydrogel electrolyte-Zn interface and alkaloid additive enables reversible and durable Zn anodes. *Chem. Eng. J.* **2024**, *497*, 154787. DOI
101. Wang, Y.; Wang, Z.; Pang, W. K.; et al. Solvent control of water O-H bonds for highly reversible zinc ion batteries. *Nat. Commun.* **2023**, *14*, 2720. DOI PubMed PMC
102. Wu, K.; Cui, J.; Yi, J.; et al. Biodegradable gel electrolyte suppressing water-induced issues for long-life zinc metal anodes. *ACS. Appl. Mater. Interfaces.* **2022**, *14*, 34612-9. DOI
103. Wood, K. N.; Kazyak, E.; Chadwick, A. F.; et al. Dendrites and pits: untangling the complex behavior of lithium metal anodes through operando video microscopy. *ACS. Cent. Sci.* **2016**, *2*, 790-801. DOI PubMed PMC
104. Jana, A.; Woo, S. I.; Vikrant, K. S. N.; García, R. E. Electrochemomechanics of lithium dendrite growth. *Energy. Environ. Sci.* **2019**, *12*, 3595-607. DOI
105. Cui, Y.; Ma, Y.; Zhao, Z.; et al. Ionic buffer layer design for stabilizing Zn electrodes in aqueous Zn-based batteries. *Mater. Rep. Energy.* **2024**, *4*, 100292. DOI
106. Argoul, F.; Freysz, E.; Kuhn, A.; Léger, C.; Potin, L. Interferometric characterization of growth dynamics during dendritic electrodeposition of zinc. *Phys. Rev. E.* **1996**, *53*, 1777-88. DOI
107. Dai, H.; Yuan, B.; Bai, C.; Lai, C.; Wang, C. Communication - direct observation of the shuttle phenomenon in lithium-sulfur batteries via the digital holographic method. *J. Electrochem. Soc.* **2018**, *165*, A2866-8. DOI
108. Chen, Y.; Li, X.; Lian, J.; et al. In situ visualization of ion transport processes in aqueous batteries. *ACS. Appl. Mater. Interfaces.* **2024**, *16*, 42321-31. DOI
109. Tian, P.; Gao, Y.; Huang, S.; et al. Constructing gradient separator to stabilize Bi-electrodes toward high-performance Zn metal batteries. *Adv. Energy. Mater.* **2024**, *14*, 2401830. DOI
110. Wu, H.; Yan, W.; Xing, Y.; et al. Tailoring the interfacial electric field using silicon nanoparticles for stable zinc-ion batteries. *Adv. Funct. Mater.* **2023**, *34*, 2213882. DOI
111. Cui, Y.; He, Y.; Yu, W.; Shang, W.; Yu, J.; Tan, P. Tailoring the electrochemical deposition of Zn by tuning the viscosity of the liquid electrolyte. *ACS. Appl. Mater. Interfaces.* **2023**, *15*, 3028-36. DOI